Revisiting the initial sites of geomagnetic field impulses during the Steens Mountain polarity reversal

Pierre Camps, Michel Prévot, Robert Coe

▶ **To cite this version:**

Pierre Camps, Michel Prévot, Robert Coe. Revisiting the initial sites of geomagnetic field impulses during the Steens Mountain polarity reversal. Geophysical Journal International, 1995, 123 (2), pp.484-506. 10.1111/j.1365-246X.1995.tb06867.x . hal-03839494

HAL Id: hal-03839494
https://hal.science/hal-03839494v1

Submitted on 4 Nov 2022

HAL is a multi-disciplinary open access archive for the deposit and dissemination of scientific research documents, whether they are published or not. The documents may come from teaching and research institutions in France or abroad, or from public or private research centers.

L'archive ouverte pluridisciplinaire **HAL**, est destinée au dépôt et à la diffusion de documents scientifiques de niveau recherche, publiés ou non, émanant des établissements d'enseignement et de recherche français ou étrangers, des laboratoires publics ou privés.

Geophys. J. Int. (1995) **123**, 484–506

Revisiting the initial sites of geomagnetic field impulses during the Steens Mountain polarity reversal

Pierre Camps,[1] Michel Prévot[1] and Robert S. Coe[2]

[1]*Laboratoire de Géophysique et Tectonique, Université de Montpellier 2, URA CNRS 1760, 34095 Montpellier Cédex 05, France*

[2]*Earth Sciences Department, University of California, Santa Cruz, CA 95064, USA*

Accepted 1995 May 18. Received 1995 April 19; in original form 1994 November 15

SUMMARY

We present a new palaeomagnetic investigation of the two sites from the Steens Mountain (Oregon) volcanic record of a Miocene polarity reversal which were supposed to record very fast changes of the geomagnetic field or impulses (Mankinen *et al.* 1985; Prévot *et al.* 1985a,b). Approximately 130 cores were first drilled from the two initial sites, belonging to sections A and B, in order to obtain at least one detailed and complete vertical sampling of each lava flow. Thermal analyses of natural remanent magnetization, complemented by some alternating field treatments, low-field thermomagnetic curves, microscopic observations and electron probe analyses of key magnetic phases, lead us to somewhat different conclusions for the first and the second impulses. At site B (first impulse), we find that the dependence of the remanence direction on the sample vertical position in flow B51 does not imply a directional field change during flow cooling, but is better explained by a thermochemical overprinting due to the overlying B50 flow. However, this conclusion does not challenge the existence of the first impulse because this field change seems to be recorded some 25 m away in flow B51 (Coe & Prévot 1989), at a place where it is thick enough for this record not to have been erased by the baking due to B50. Regarding the second impulse, restudied at site A, our new findings are more comprehensively explained by a change in the field direction during cooling of flow A41-2 than by some overprinting. Using a simple model of flow cooling, the angular rate of change of the field is estimated to have been of the order of 2°–3° or 250–350 nT per day during the impulse. This figure is similar to that previously obtained from site D, some 250 m away. However, the directional paths describing the field change are somewhat different at the two sites. New investigations are planned to try to understand the origin of this discrepancy.

Key words: geomagnetism, palaeomagnetism, polarity reversals.

1 INTRODUCTION

How the geomagnetic field reverses its polarity is one of the most intriguing questions in geophysics. Among the large number of observations from volcanic and sedimentary rocks relating to this problem, the very fast field changes that have been suggested to occur twice during the Miocene R-N reversal (Mankinen *et al.* 1985; Prévot *et al.* 1985a; Coe & Prévot 1989) recorded by the Steens Basalt (Oregon) are probably the most challenging observations for understanding the reversal process. Each of these very fast field changes, or 'impulses', is associated with a large directional gap (some 90°) in the record and is partially recorded within a single flow. Within these flows, the cleaned direction of remanence is found to vary largely along a vertical section. In the best-documented example so far published (Coe & Prévot 1989), both the bottom and the upper parts of the flow exhibit directions close to that of the underlying flow (pre-gap direction) whereas the interior shows directions tending towards that of the overlying flow (post-gap direction).

As the bottom and the upper parts of a lava flow cool faster than the interior, the hypothesis that the field was changing in direction during the flow cooling qualitatively accounts for the observed trend in direction. A more rigorous test has recently been carried out for the second impulse (Camps, Prévot & Coe 1995) by combining the palaeomagnetic data with cooling-time estimates as obtained from a simple numerical cooling model of lava flows. The angular speed of field change is then found to be $6° \pm 2°$ per day, which is similar to a more approximate estimate previously given for the first impulse

© 1995 RAS

Downloaded from http://gji.oxfordjournals.org/ at ISTEEM /Institut des Sciences de la Terre de l'Eau et de l'Espace de Mont on February 19, 2013

(Coe & Prévot 1989). Such a figure is large compared to the rate of change of the present field (Langel & Estes 1985), even when the difference in field magnitude is taken into account (Prévot *et al.* 1985b). For comparison, field rotations amounting to 0.5° per year have been reported for palaeosecular variation from the study of Eocene flows (Nyblade, Shive & Furlong 1987). Very high velocities, of the order of 1 km hr^{-1}, might be needed at the top of the liquid core to generate the very rapid field changes of the Steens Mountain record (Coe & Prévot 1989).

On the other hand, it is obvious that the vertical distribution of remanence directions cannot be explained by a simple heating caused by the overlying post-gap flow. Also, the detailed rock magnetic experiments carried out on those 'impulsive' flows (Coe & Prévot, in preparation), which are partially summarized in Coe, Prévot & Camps (1995), do not favour an interpretation involving a remagnetization process such as suggested by Fuller (1989). Other alternative explanations (for example, multiple magmatic injections within these flows), either can be ruled out or do not modify the order of magnitude of the estimated rate of change of the field (Coe *et al.* 1995).

However, the hypothesis of impulsive field changes poses several difficulties. First, their origin is still unclear. An external origin is difficult to reconcile with the fact that these changes occur between two relatively long-lived field directions which, because of their time constant, must be of internal origin (Coe & Prévot 1989). An internal origin of the fast field changes is dismissed by many geomagnetists because the velocity at the top of the core would have to be of the order of 1 km hr^{-1} (Coe & Prévot 1989), which is three orders of magnitude larger than deduced from the present field. Also, most of the electrical conductivity models of the mantle would not allow such a rapid signal to have travelled through the entire mantle due to electromagnetic filtering (Gubbins & Roberts 1987). However, this point of view can be challenged in the light of

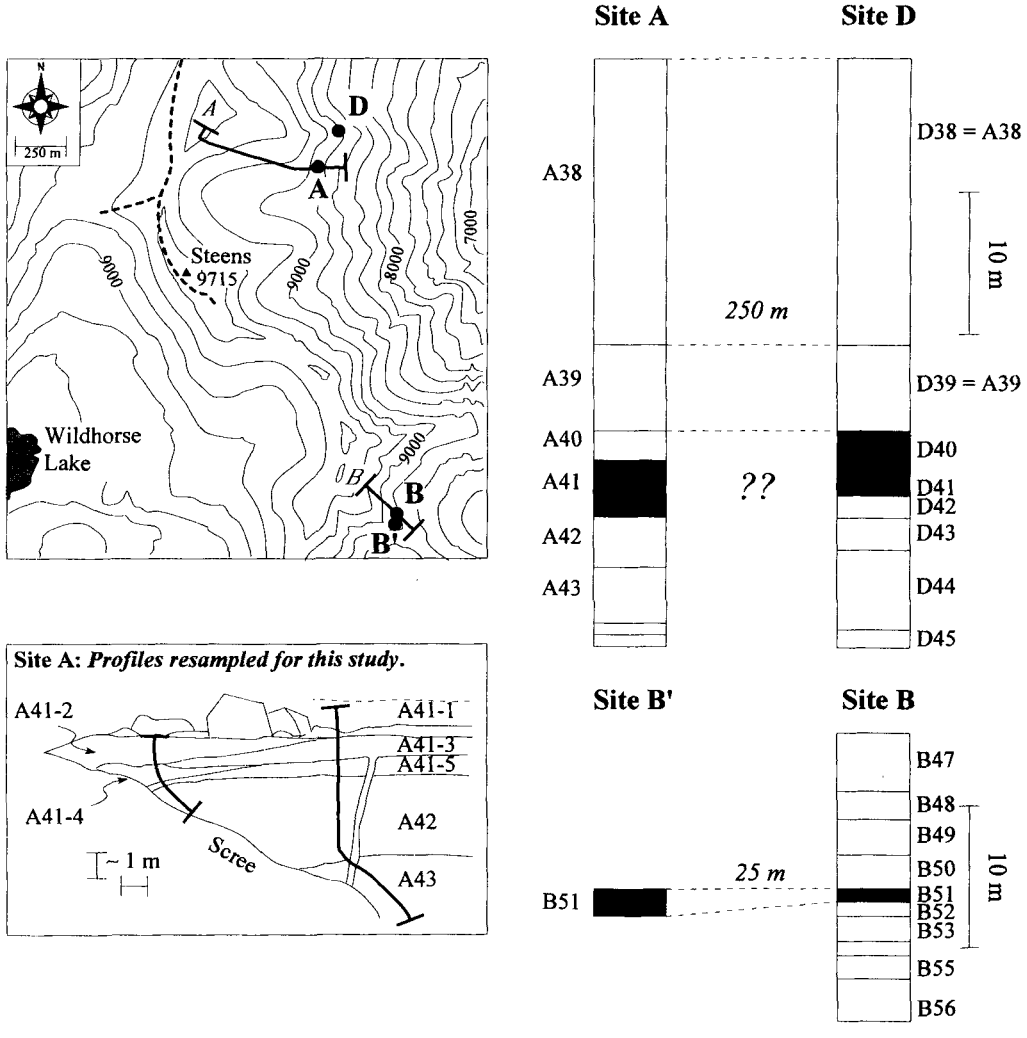

Figure 1. Sketch showing locations of sampled sections (upper left). Solid lines show locations of sections *A* and *B* of Mankinen *et al.* (1985). Solids dots denote the approximate location of the sites A, B, B′ and D where the flows, which have suggested the geomagnetic impulses, have been resampled. The first impulse is studied at site B (this study) and site B′ (Coe & Prévot 1989); the second one at site A (this study and Prévot *et al.* 1985) and site D (Coe *et al.* 1995; Camps *et al.* 1995). Profiles of the lava sequence at each site are shown on the right. Shading denotes the unusually magnetized flows. The stratigraphic organization of the flows located at the level of the second jump at site A is shown on a schematic cross-section (lower left).

Downloaded from http://gji.oxfordjournals.org/ at ISTEEM /Institut des Sciences de la Terre de l'Eau et de l'Espace de Mont on February 19, 2013

Table 1. Pre- and post-gap directions and palaeointensities (when available) recorded at site B of the first impulse and site A of the second impulse.

Impulse	Flow #	Thickness (m)	Cleaning method	n / N	I	D	k	α_{95}	Fe ± sd (μT)	Ref.
2^{nd} : *post-gap directions*	A38	22.0	AF + Th	8 / 10	36.6	140.0	182	4.1	13.2 ± 1.0	1, 2
	A39	6.0	AF + Th	9 / 9	38.6	140.8	199	3.7	8.7 ± 3.0	1, 2
	A40	2.0	AF + Th	3 / 4	36.0	137.0	—	—	4.4 ± 0.3	1, 2
2^{nd} : *pre-gap directions*	A41-3	1.2	Th	12 / 12	48.3	274.4	857	1.6	—	3
	A41-4	1.1	Th	15 / 15	45.5	277.5	70	4.8	—	3
	A41-5	0.7 - 0.9	Th	15 / 15	44.1	279.4	573	1.6	—	3
	A42	3.5	AF	8 / 8	52.6	270.5	39	8.9	7.0 ± 1.1	1, 2
	//	3.0	Th	8 / 8	37.4	275.8	76	6.4	—	3
	A43	3.9	AF + Th	8 / 8	48.0	278.0	299	3.2	—	1
	//	3.9	Th	20 /21	47.8	273.8	74	3.8	—	3
1^{st} : *post-gap directions*	B50	2.4	AF	7 / 8	57.3	330.5	113	5.7	—	1
1^{st} : *pre-gap directions*	B52	1.0	AF	4 / 6	32.6	146.6	319	5.2	—	1
	//	0.9	Th	6 / 7	31.9	153.1	117	6.2	—	3
	B53	1.8	AF	8 / 8	42.4	143.6	125	5.0	—	1
	B54	1.0	AF	7 / 7	29.1	142.4	186	4.4	5.8 ± 2.8	1, 2
	B55	1.6	AF	5 / 6	39.3	143.1	181	5.7	—	1
	B56	3.0	AF	6 / 7	33.1	144.1	312	3.8	—	1
	B57	1.0	AF	4 / 4	36.6	144.9	311	5.2	—	1
	B58	0.4 - 2.0	AF	2 / 2	42.0	136.0	—	—	—	1

(1) Mankinen *et al.* (1985); (2) Prévot *et al.* (1985); (3) this study

n/N, number of samples used in the analysis/total number of samples collected; *I*, inclination positive downward; *D*, declination east of north; k, precision parameter; α_{95}, 95 per cent confidence cone about average direction; Fe ± sd, unweighted average palaeointensity of individual lava flow—the plus and the minus sign corresponds to the standard error.

some recent experimental data and models concerning mantle conductivity (Coe *et al.* 1995). A second difficulty is that the probability for a volcanic eruption to occur simultaneously with such a rapid field change (estimated to have lasted for two weeks or so) is very small, unless such jumps occur very frequently during reversals (Coe *et al.* 1995). Given the present state of this debate, we re-examined the initial sites from the study in which the hypothesis of very fast field changes was proposed, and report here the results of this new investigation.

2 GEOLOGY AND SAMPLING

The magnetic study of the lava flows suspected to have recorded fast field changes was carried out in three steps. The initial analyses (Mankinen *et al.* 1985; Prévot *et al.* 1985a,b) relate to flows belonging to the Steens Mountain *A* and *B* sections (Fig. 1), sampled in 1977 and 1981. A second set of studies deals with two sites laterally distinct from the initial sites (which will be called simply site A and site B in the present paper). The two additional sites, sampled in 1985, are site B′ (Coe & Prévot 1989) located 25 m south of site B, and site D (Coe *et al.* 1995; Camps *et al.* 1995) located 250 m north of site A (Fig. 1). We present here also a new study of sites A and B, which were resampled in 1985.

The first and second geomagnetic impulses were initially described from flows B51 (along section *B*) and A41 (section *A*) respectively. In contrast to the initial 1977 and 1981 samplings, the 1985 sampling was very detailed along several vertical sections. Flow B51 was vertically resampled at site B, where it is approximately 90 cm thick, and sampled at site B′, where it thickens to reach 190 cm (Coe & Prévot 1989). Flow B52 was also sampled at site B, where it is about 95 cm thick, but this sampling was somewhat incomplete because of drilling problems. A total of 22 cores were drilled. These two flows are massive and rich in phenocrysts. They exhibit subhorizontal obvious bottom and top contacts and are laterally continuous from B to B′. However, flow B51 must pinch out somewhere between site B and site A, which is 1.5 km north of B, because the pre- and post-gap directions are found there in two consecutive flows directly in contact with each other. At sites B and B′, the post-gap direction is recorded by the overlying massive aphyric flow B50, which is 2.3 m thick and had been sampled in 1981 (Mankinen *et al.* 1985).

The resampling of the second impulse at site A revealed that up to five units (labelled A41-1 to A41-5), some of them pinching out only a few metres away from the two drilled sections (Fig. 1), can be recognized between A42 (which provides the pre-gap direction, as we will show below) and the overlying A40 flow which records the post-gap direction (Mankinen *et al.* 1985). Units A41 are thin (their composite thickness is 4.0 m) and constitute altogether a typical compound lava flow (Walker 1970). They probably correspond to a single volcanic eruption, possibly having lasted between some hours and a few months (G. P. Walker, private communication). These units are aphyric, vesicular near the bottom and top, and their surface is typical of pahoehoe flows. Each of them shows a simple structure, with no indication of late magmatic injections (G. P. Walker, private communication). Altogether, 49 cores were sampled in these units along two sections a few metres apart (Fig. 1). The pre-gap flow A42, which is 3.0 m thick, is massive and aphyric. It was also sampled (38 cores) over its entire thickness (Fig. 1), with the exception of the lowermost 30 cm. The lowermost flow we resampled in 1985 is the aphyric flow A43, which is 4.3 m thick. Twenty-one cores were drilled in the upper 3 m of this flow.

Downloaded from http://gji.oxfordjournals.org/ at ISTEEM /Institut des Sciences de la Terre de l'Eau et de l'Espace de Mont on February 19, 2013

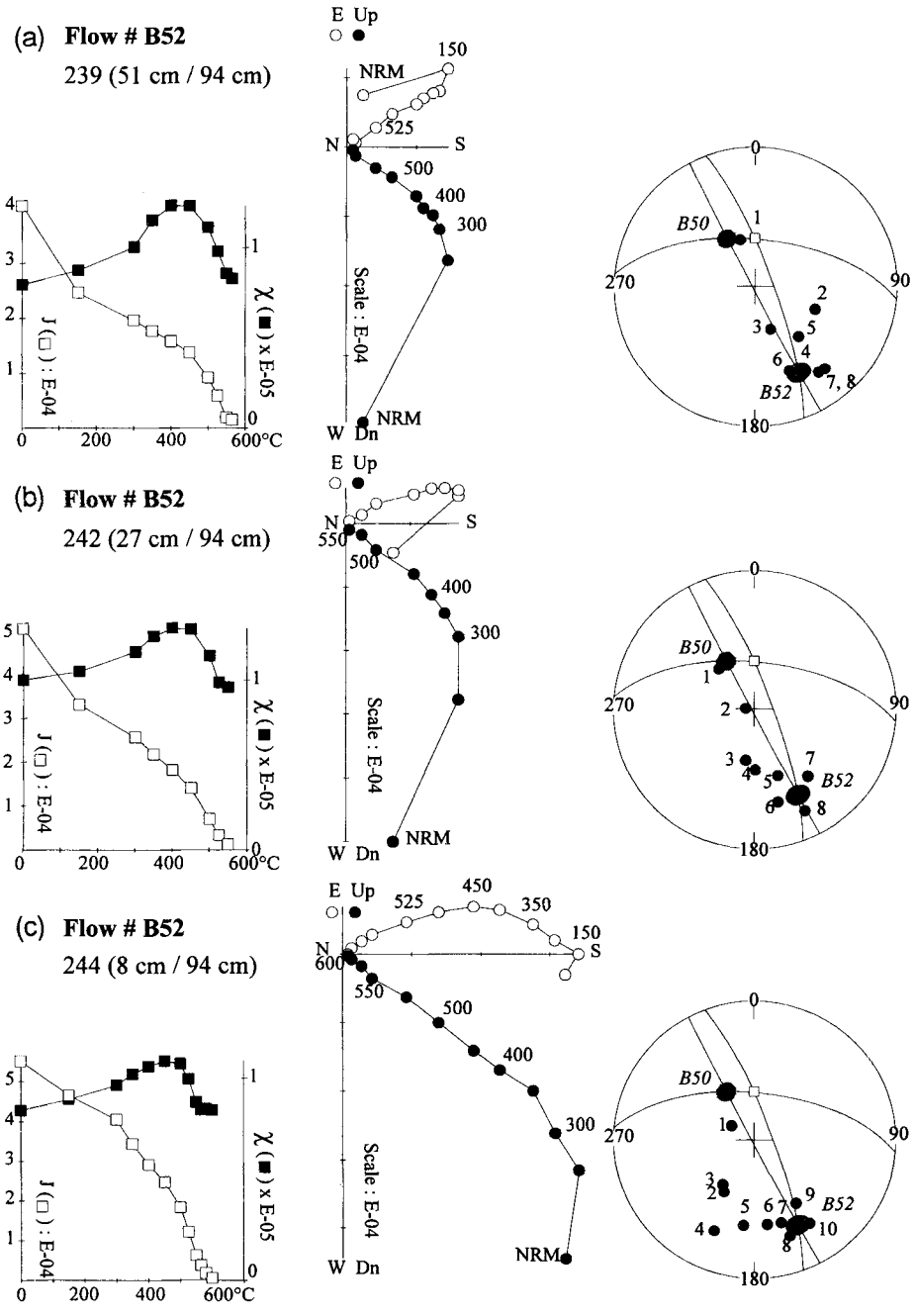

Figure 2. Thermal demagnetization of NRM (left column, □), room-temperature susceptibility versus heating temperature (left column, ■), orthogonal diagrams of progressive thermal demagnetization of NRM (middle column) and vector differences shown on an equal-area projection (right column) for samples from (a) the top, (b) the middle and (c) the bottom of flow B52. The core number should, for example, be read 85P239 instead of 239 (the same rule has been used for all figures). The core number is followed (within brackets) by the distance of the core from the lava flow bottom contact and the flow thickness. Units of the variation of NRM intensity and susceptibility are $Am^2\ kg^{-1}$ and $m^3\ kg^{-1}$, respectively. On the orthogonal diagrams, filled circles correspond to the projection onto the vertical plane while open symbols are projection onto the horizontal plane. On the equal-area projection, filled and open circles represent positive and negative inclinations, respectively. Great circles containing the before (B52), and after (B50) jump directions (measured by Mankinen *et al.* 1985) and normal axial dipole field direction (□) are drawn. Labelled numbers by the dots increase with the heating temperature.

The three flows overlying A41, sampled in 1977, are highly porphyritic and yield the same direction of remanence corresponding to directional group 21 (Mankinen *et al.* 1985). A baked aeolian deposit, 1–2 cm thick, lies between flows A40 and A39. A similar aeolian deposit is probably also present at the A40/A41 boundary. At site A, this contact is hidden by rubble but, a few hundred metres away, both north and south of the present site, a distinctive aeolian deposit 2–5 cm thick could be observed. Thus, some time elapsed between the emplacement of each of these three flows. Furthermore, the palaeointensity found from flows A38 and A37 (Prévot *et al.* 1985b) is significantly higher than for the underlying flows,

Downloaded from http://gji.oxfordjournals.org/ at ISTEEM /Institut des Sciences de la Terre de l'Eau et de l'Espace de Mont on February 19, 2013

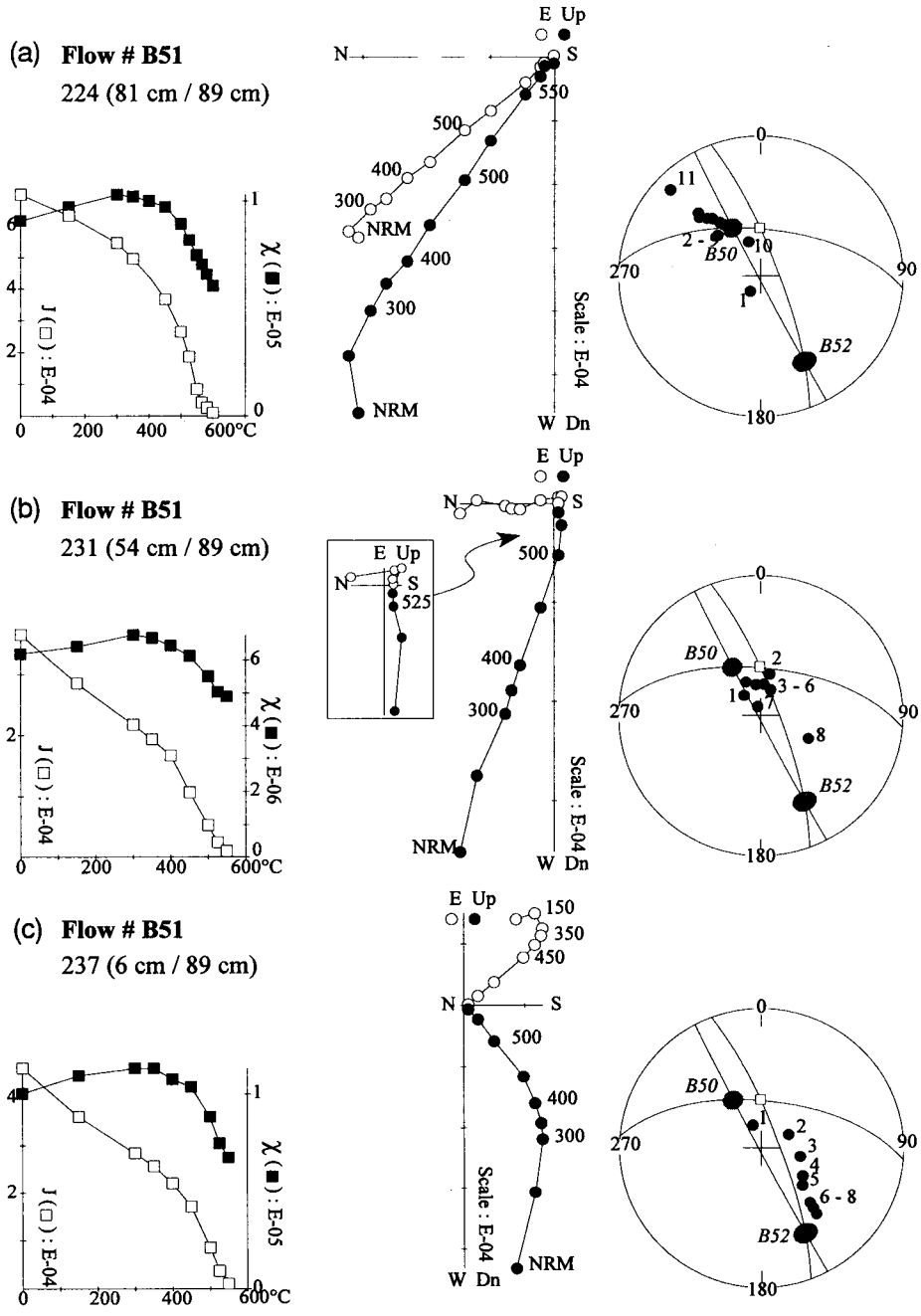

Figure 3. Thermal demagnetization of NRM (left column, □), room-temperature susceptibility versus heating temperature (left column, ■), orthogonal diagrams of progressive thermal demagnetization of NRM (middle column) and vector differences shown on an equal-area projection (right column) for samples from (a) the top, (b) the middle and (c) the bottom of flow B51. Same representation as in Fig. 2.

which suggests another eruptive gap before A38 was emplaced. Thus, flows A40, A39 and A38 did not cool simultaneously. The thicknesses of the overlying flows are 2 m (A40), 6 m (A39) and 22 m (A38), with large variations in the relative thickness of the first two units from place to place.

3 EXPERIMENTAL PROCEDURES

If a rapid change in the direction of the field occurs during the cooling of a lava flow, the thermoremanent magnetization (TRM) acquired is the sum of partial TRMs (PTRMs), each of them recording a specific field direction depending on the time interval during which magnetization was blocked. Thus, under the hypotheses that the primary remanence is a TRM and that blocking and unblocking temperatures are the same, the progressively changing direction of the palaeofield can be determined from the vector differences between successive thermal demagnetization steps. To achieve a good precision, we used 14–17 cleaning steps for each specimen, with temperature intervals sometimes as small as 15 °C. The oven, manufactured by Pyrox, is non-inductive and is located in a field-free space (residual magnetic flux density less than 20 nT). The temperature at the centre of the specimen is known with a ± 5 °C precision. Note that to eliminate short time-constant

Downloaded from http://gji.oxfordjournals.org/ at ISTEEM /Institut des Sciences de la Terre de l'Eau et de l'Espace de Mont on February 19, 2013

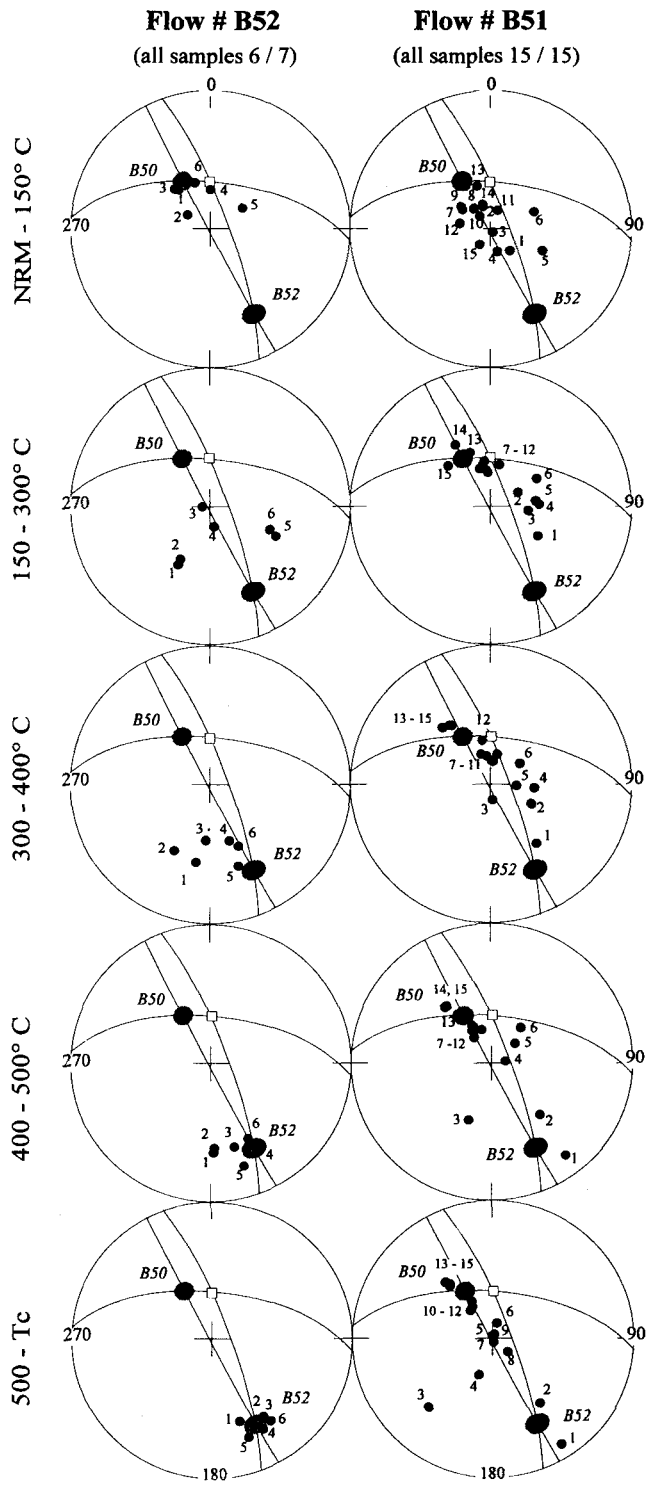

Figure 4. Equal-area projection of directions of vector differences calculated for different temperature intervals for all samples from flows B52 (left column) and B51 (right column). On this figure the cores have been given numbers 1 to 15, starting from the base of the flow and increasing upwards. The numbering starts from 1 and increases upward. Filled and open circles represent positive and negative inclinations respectively. Other directions as in Fig. 2.

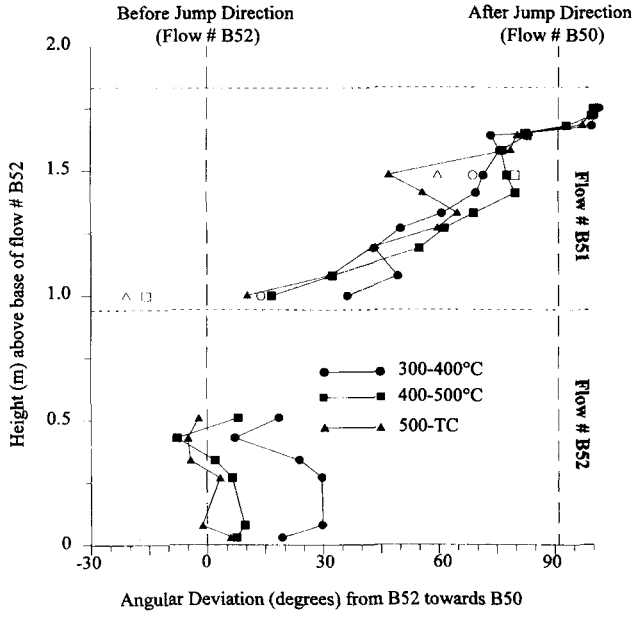

Figure 5. Angular deviation of remanence calculated for different unblocking-temperature intervals for samples from flows B52 and B51 as a function of their height above the base of flow B52. Each palaeodirection is projected on to the great circle containing the pre- and post-jump directions, the angular deviation being measured along this great circle from the pre-jump direction towards the post-jump direction. Open symbols correspond to samples that were collected a few centimetres away from the main vertical section of sampling.

VRM (viscous remanent magnetization), the specimens had been stored in a field-free space for at least three weeks before thermal demagnetization was undertaken. In order to minimize magneto-chemical changes, each temperature step was maintained for 15 min only. To try to detect such changes, low field susceptibility was measured at room temperature after each heating step.

Precise measurements of remanence were obtained using a CTF cryogenic magnetometer with an application code which permitted plotting of magnetization changes in real time (Levêque 1992). This facility proved to be extremely useful because the remanence of a few specimens became very unstable after demagnetization at temperatures higher than 400 °C, with relative changes amounting to 25 per cent over 50 min in the worst case. This instability is probably due to spurious magnetizations acquired in the laboratory field during the transfer of the specimen from the oven into the magnetometer. For most specimens, however, this change was less than 5 per cent. All the measurements were recorded only after stabilization of remanence in the cryogenic magnetometer, which sometimes required waiting for a few tens of minutes.

4 DESCRIPTION OF THE FIRST DIRECTIONAL GAP

Let us recall first that the pre-gap field direction was certainly constant for a long time, as it is recorded by seven consecutive flows (B52 to B58), some aphyric and others porphyric, constituting directional group 31 (Mankinen *et al.* 1985). Flow B54 provided a very small field palaeointensity, equal to 5.8 ± 2.8 μT (Prévot *et al.* 1985b). In contrast, a single flow (B50) records the post-gap direction (Table 1).

Downloaded from http://gji.oxfordjournals.org/ at ISTEEM /Institut des Sciences de la Terre de l'Eau et de l'Espace de Mont on February 19, 2013

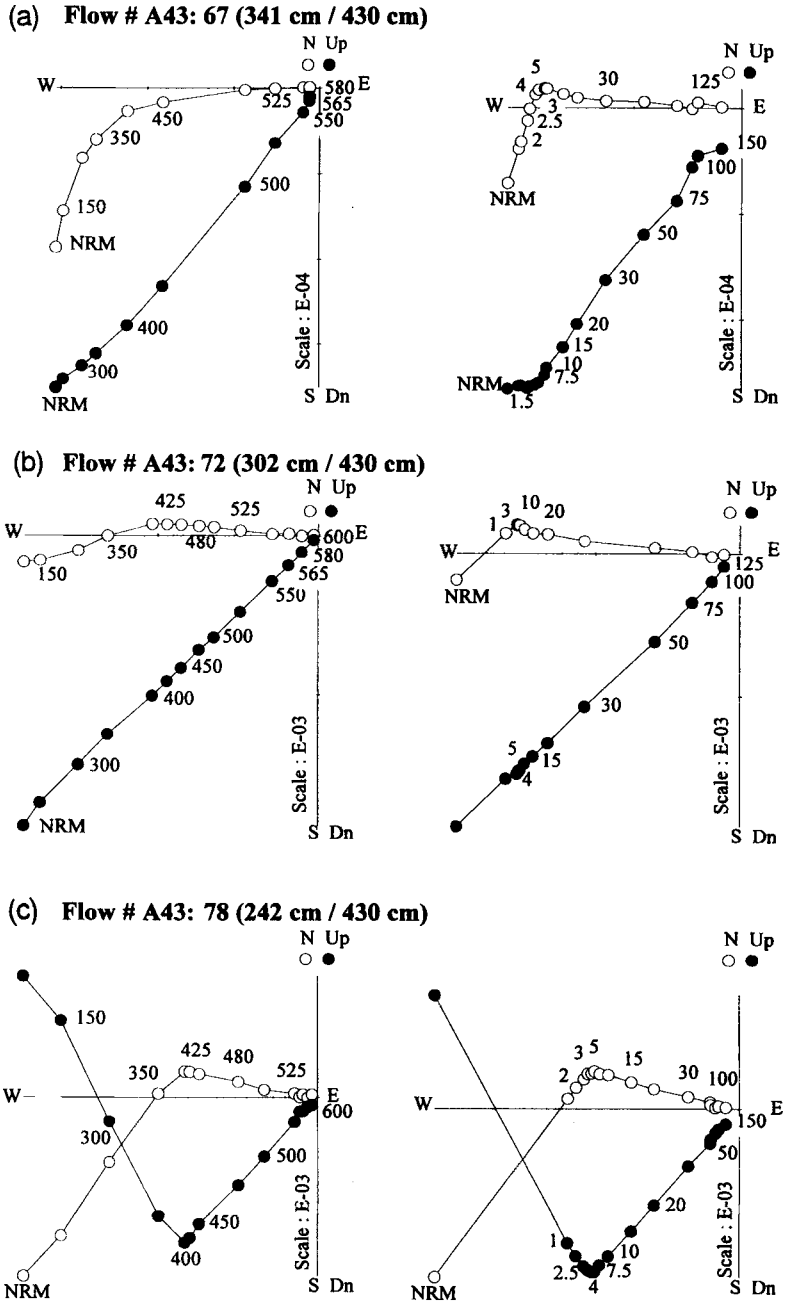

Figure 6. Flow A43. Orthogonal diagrams of progressive thermal (left column) and alternating field (right column) demagnetization of NRM. Same symbols as in Fig. 2.

The present sampling of flows B52 and B51 consisted of rather short cores due to drilling problems in the field. Only directional magnetic studies could be carried out with the available material. The results from thermal analyses are shown for a few representative specimens (Figs 2 and 3), using orthogonal plots and an equal-area azimuthal projection, and for all specimens in each flow (Fig. 4), as a sequence of azimuthal projections corresponding to successive temperature intervals. Moreover, following the representation of Coe & Prévot (1989), Fig. 5 shows for both flows the angular progression of the direction of the difference vectors for successive temperature intervals for each core, measured from the underlying (B53) flow direction towards the overlying (B50) flow direction, and plotted as a function of the core height above the base of B52.

4.1 Flow B52

To a first approximation, the directions of remanence are similar, in each temperature interval, regardless of the vertical position of the core in the flow. In particular, the high-temperature directions are well clustered (Fig. 4) with a precisely defined average which agrees with the previous estimate obtained from AF demagnetization of the 1977 collection and is only slightly different from the direction of the underlying B53 lava flow (Table 1). The 500 °C-T_c directions are not

Downloaded from http://gji.oxfordjournals.org/ at ISTEEM /Institut des Sciences de la Terre de l'Eau et de l'Espace de Mont on February 19, 2013

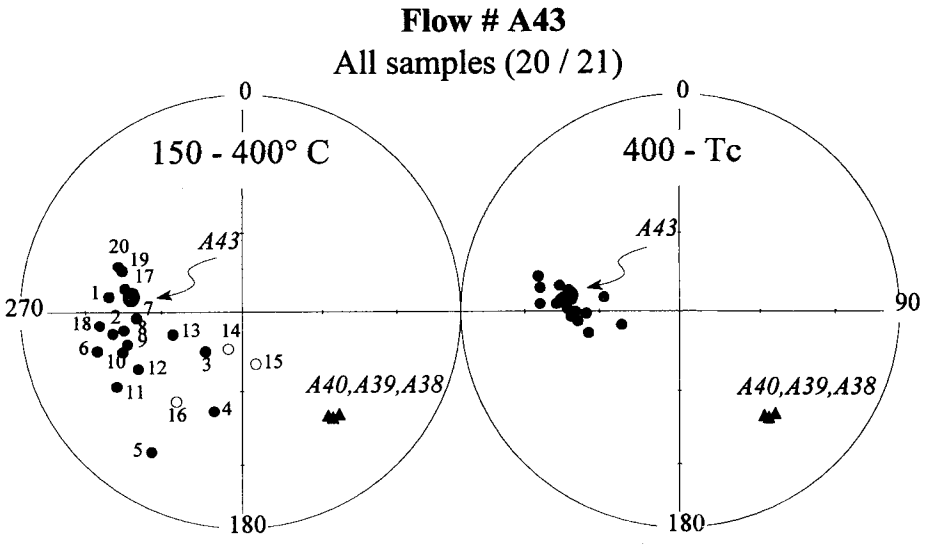

Figure 7. Equal-area projection of the two components of magnetization found in flow A43 (same diagrams as in Fig. 4). The pre-jump direction (flow A43) and the post-jump directions (flows A40,39,38) measured by Mankinen *et al.* (1985) are represented.

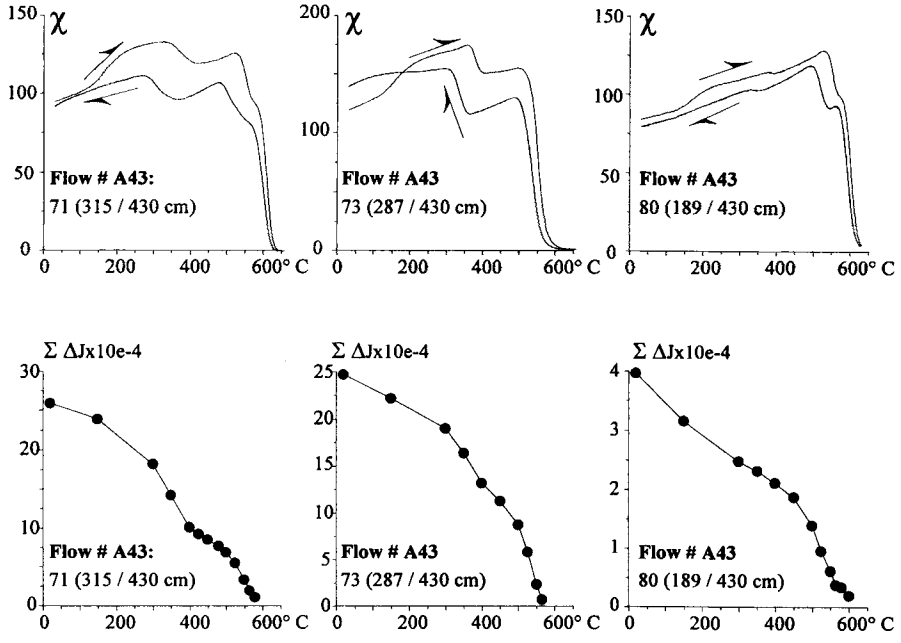

Figure 8. Thermal dependence of weak field magnetic susceptibility χ under vacuum and sum of partial remanence intensities for three samples from flow A43. Heating and cooling curves are indicated by arrows. Note the presence of three main magnetic phases in this flow, with Curie points close to 370, 580 and 630 °C.

significantly dependent upon the core height (Figs 4 and 5). They constitute the latest record of the pre-gap field direction.

In the lowest temperature interval (20–150 °C), quite a large remanence is destroyed, especially near the flow centre (Fig. 2), with directions close to those of both the axial dipole field and the direction of the post-gap flow B50, which barely differ from each other (Fig. 4). Measurements of the viscosity index v (Thellier & Thellier 1944) indicate that the 15-day VRM increases steadily from the flow bottom ($v = 5$ per cent) towards the flow centre ($v = 13$ per cent), which nicely parallels the increase of the low-T component. For subaerial lava flows, it has been found that the Brunhes VRM is, on average, three times larger than the two-week VRM (Prévot 1975). When combined with the values found for v, this figure provides for each sample a magnitude estimate for the Brunhes VRM which is quite close to the magnitude of the low-T components. Thus, this component corresponds very probably to a viscous overprint acquired in the recent field. We suggest that the change in direction of the difference vectors as T increases (Fig. 4) basically reflects the progressive decrease of the *in situ* VRM. Given the importance of VRM in these specimens, the small change in direction with height seen for the 300–400 °C temperature interval (Fig. 5) has probably no significance in terms of the direction of the non-viscous remanence.

There is some evidence that the difference vectors for intermediate temperatures deviate slightly but significantly from the great circle joining the high-temperature pre-gap direction to the dipole field direction (Fig. 5). This second-order obser-

Downloaded from http://gji.oxfordjournals.org/ at ISTEEM /Institut des Sciences de la Terre de l'Eau et de l'Espace de Mont on February 19, 2013

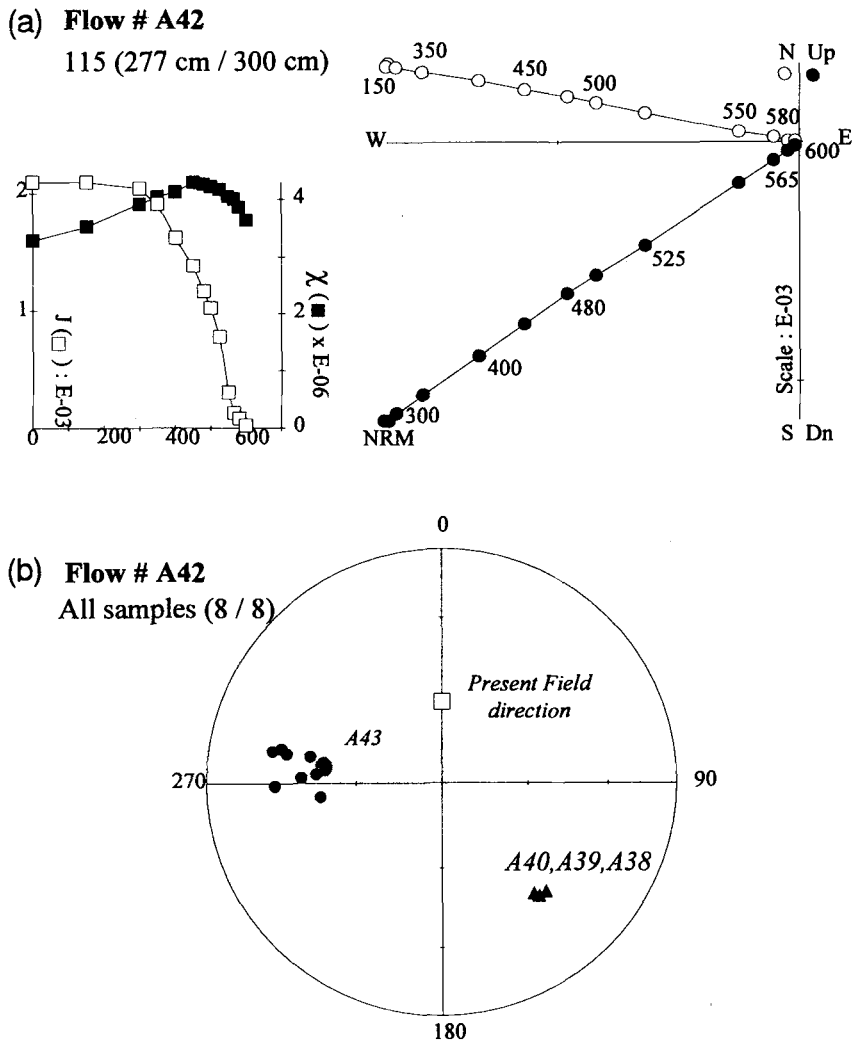

Figure 10. Thermal demagnetization of NRM of flow A42: (a) diagrams as in Fig. 2; (b) diagrams as in Fig. 7. In this flow, only one magnetization component, corresponding to the pre-jump direction, is found.

vation is difficult to explain. A small westward-movement of the field during the lava flow cooling is a possibility, but this is not verifiable given the weakness of observational constraints.

4.2 Flow B51

For most of the 15 cores drilled, with the noticeable exception of the four lowermost ones (within 25 cm of the bottom contact), the directions of the difference vectors are generally similar, for each core, in the various temperature intervals (Figs 3 and 4). However, the magnetic directions change progressively, and almost linearly, with the vertical position of each core within the flow (Fig. 5), moving approximately along the great circle between the pre- and post-gap directions (Fig. 4). The angular distance from the pre-gap direction recorded in B52 varies approximately from 50° at 25 cm from the lower contact to 100° at the flow top, which corresponds to a direction close to that of the overlying flow, although exceeding it by some 15°, as already observed at site B′ (Coe & Prévot 1989).

The two cores drilled at 14 and 25 cm from the flow bottom exhibit a fairly constant direction of difference vectors up to 450 °C, a behaviour similar to that just reported for the cores higher in the flow. Beyond this temperature, however, the direction moves to a south-west declination (Fig. 3c), which presents some analogy with the movement of the 300–400 °C component towards such declinations observed in flow B52. The two lowermost cores (labelled 1 and 2 in Fig. 4), collected some 5 cm apart from each other, both at 6 cm from the bottom contact, show a very progressive and large (some 90° in total) displacement of the direction of difference vectors along the great circle mentioned above (Fig. 3d). The direction, almost vertical at low T, moves continuously towards the pre-gap direction as temperature increases.

The significance of the trends in direction observed for the four lowermost cores is as unclear as for flow B52, and this for the very same reasons: the viscosity is not negligible (v varies from 7 to 11 per cent) and the recent field direction is close to the post-gap direction. Thus it is difficult to know if these changes in direction have some origin other than recent viscous overprinting.

4.3 Summary of main observations

Our main observations relative to the first directional gap can be summarized as follows.

Downloaded from http://gji.oxfordjournals.org/ at ISTEEM /Institut des Sciences de la Terre de l'Eau et de l'Espace de Mont on February 19, 2013

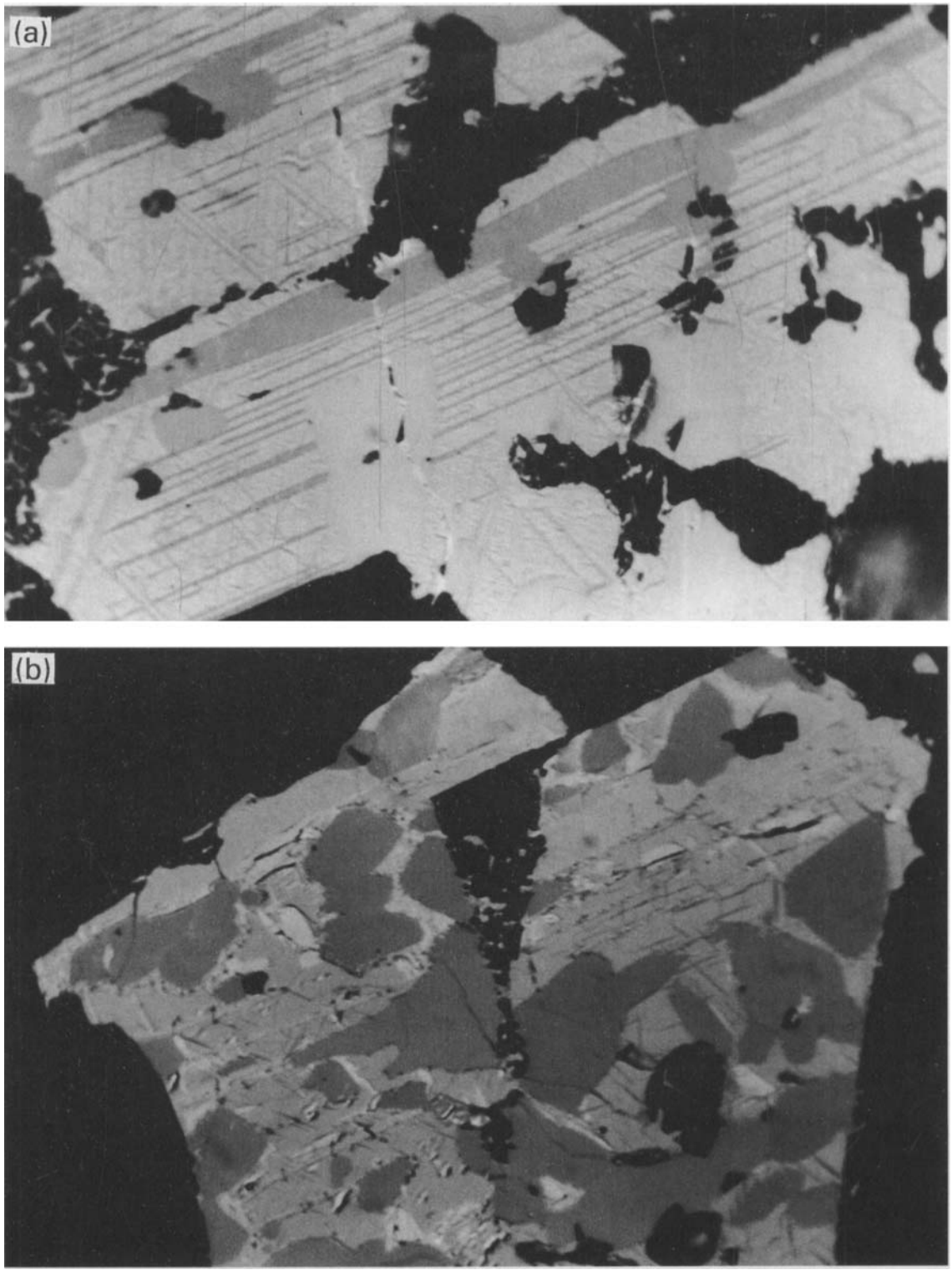

Figure 9. Reflected light microphotographs from lava flows A43 (core 85P071) and A41-3 (core 85P118). (a) A43, oil immersion, crossed nicols, dimensions 54 × 36 μm. Ilmenite intergrowths in titanomagnetite of the trellis type with some anhedral ilmenite inclusions. (b) A43, oil immersion, crossed nicols, dimensions 54 × 36 μm. Oxidized titanomagnetite–ilmenite intergrowth showing residual ilmenite (light grey), residual (titano)magnetite (medium grey) containing spinel lamellae (black), blebs of exsolved pseudobrookite (heavy grey), and titanohaematite (white). (c) A43, oil immersion, crossed nicols, dimensions 54 × 36 μm. A completely pseudomorphosed grain of titanomagnetite showing an assemblage of pseudobrookite (heavy grey) and titanohaematite (white), probably as a result of a very rapid oxidation of original titanomagnetite (Haggerty 1976). (d) A43, in air, dimensions 130 × 90 μm. Secondary magnetic minerals resulting from high-temperature oxidation of olivine (grey mottled areas) forming a composite mantle of magnesioferrite (medium grey) and titanohaematite (white). (e) A43, in air, dimensions 130 × 90 μm. Secondary minerals (magnesioferrite and titanohaematite) crystallized in proximity of olivine (near lower left corner). (f) A41-3, in air, dimensions 330 × 220 μm. Cruciform titanomagnetite crystals (near middle of flow).

Downloaded from http://gji.oxfordjournals.org/ at ISTEEM /Institut des Sciences de la Terre de l'Eau et de l'Espace de Mont on February 19, 2013

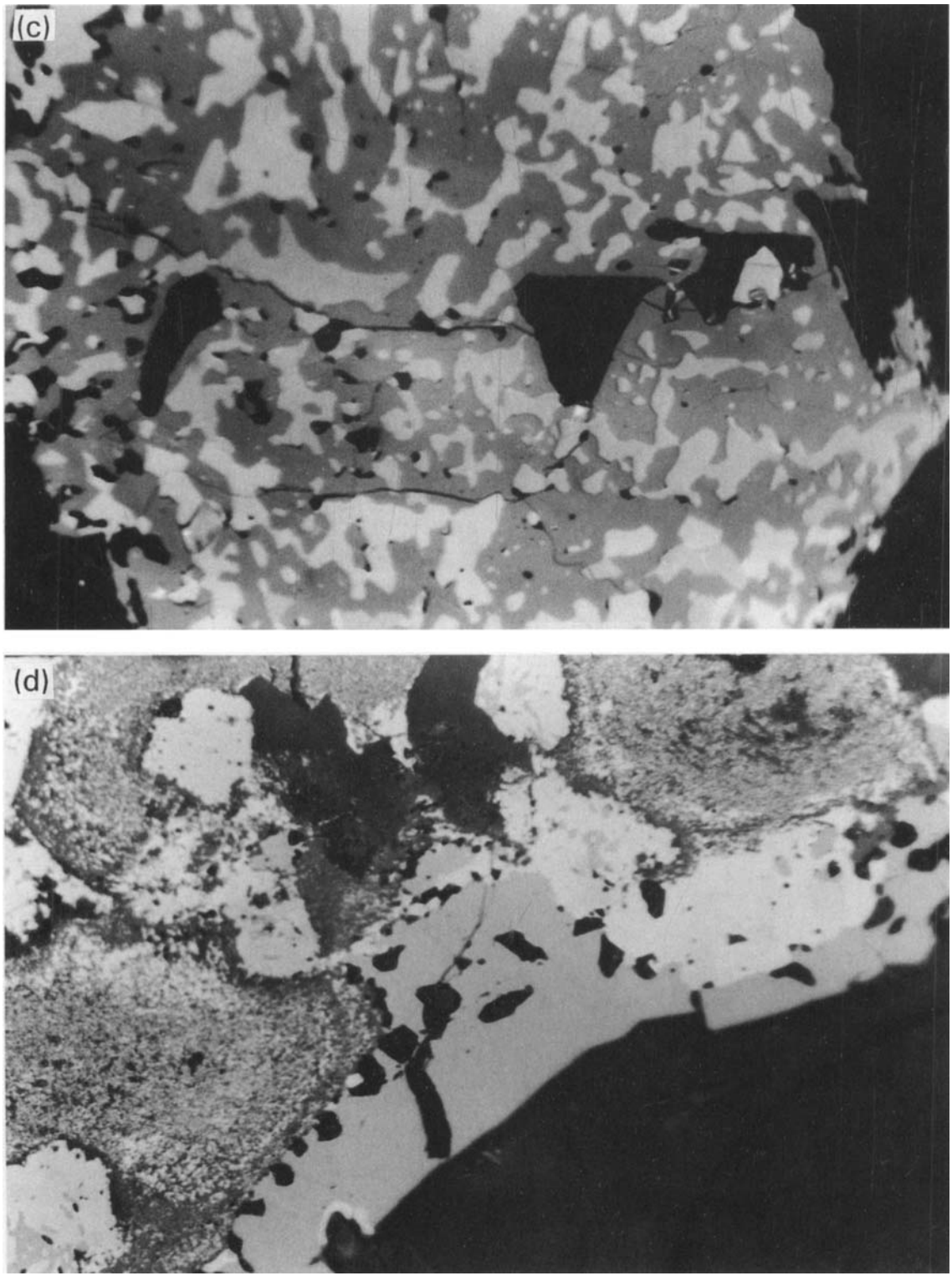

Figure 9. (*Continued.*)

Downloaded from http://gji.oxfordjournals.org/ at ISTEEM /Institut des Sciences de la Terre de l'Eau et de l'Espace de Mont on February 19, 2013

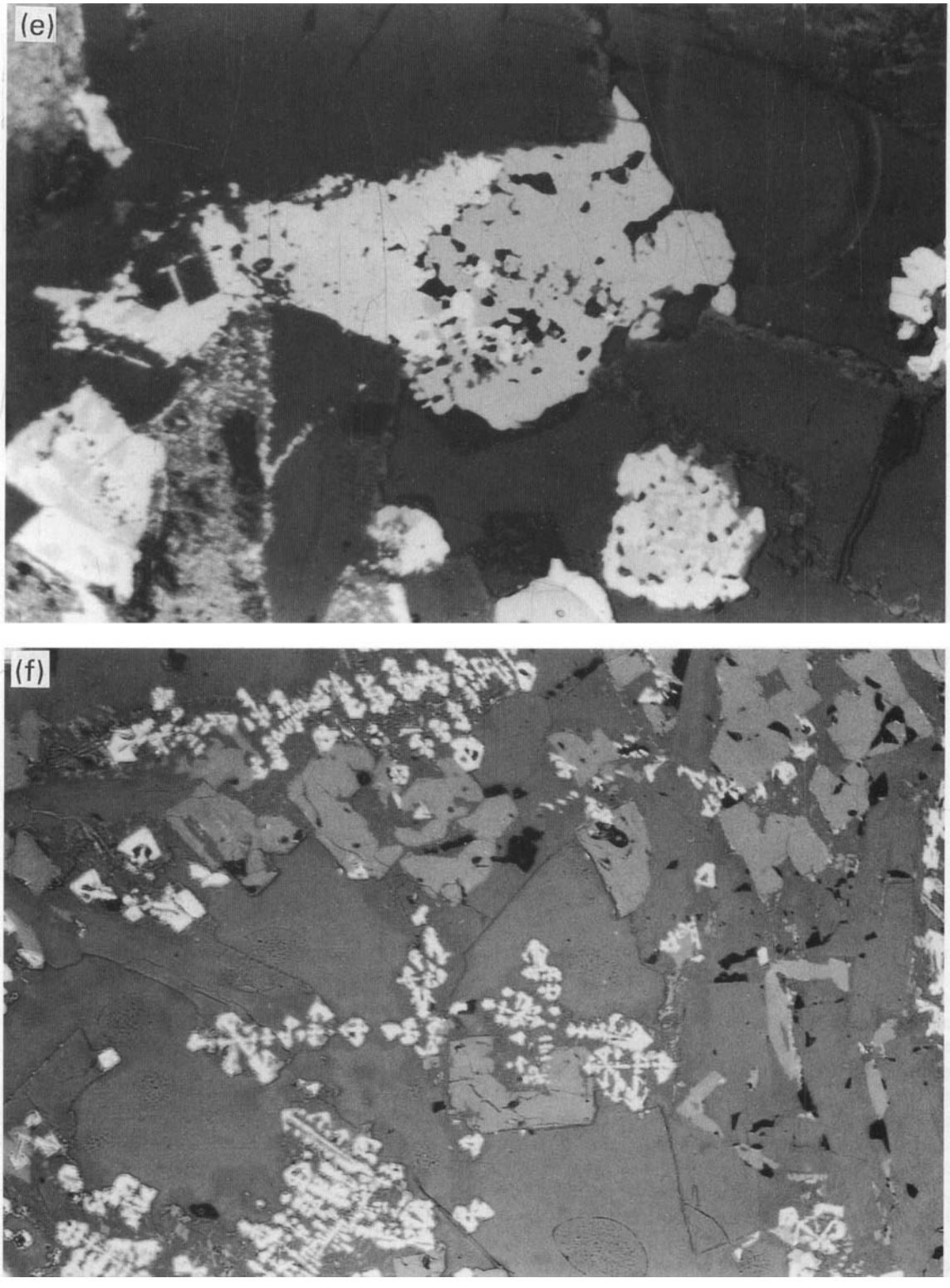

Figure 9. (*Continued.*)

Downloaded from http://gji.oxfordjournals.org/ at ISTEEM /Institut des Sciences de la Terre de l'Eau et de l'Espace de Mont on February 19, 2013

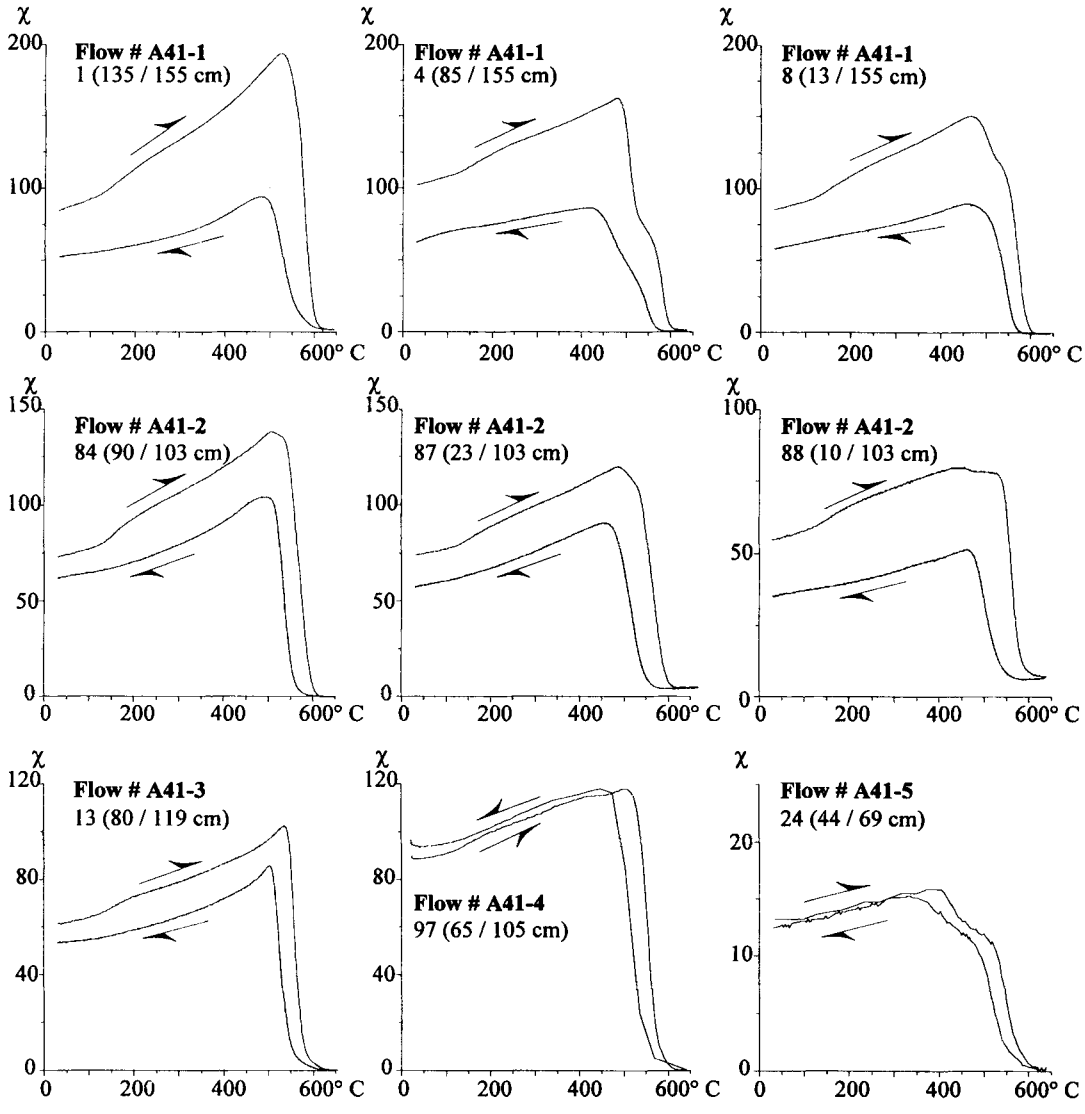

Figure 11. Thermal dependence of weak field magnetic susceptibility χ for some specimens from lava flow units A41-1 to A41-5. The magnetic mineralogy of these flows is dominated by high Curie temperature phases ($\approx$580 °C).

(1) The lower half of flow B52 (the only part of the flow sampled) shows no clear evidence of a dependence of the direction of remanence on the vertical position of the core within the flow. The thermal dependence of magnetization direction may simply reflect the progressive destruction of the large Brunhes VRM. The high-temperature direction of remanence can be interpreted as the latest record of the pre-gap field direction.

(2) In the upper 70 cm of flow B51, the direction of remanence is basically temperature-independent. In contrast, the direction is dependent on the core vertical position in the flow. When moving downwards, the direction changes progressively from the post-gap field direction, observed near the flow top, toward an intermediate direction some 50° from the pre-gap direction. For the cores closer to the flow base, the direction of magnetization is temperature-dependent.

5 DESCRIPTION OF THE SECOND DIRECTIONAL GAP

According to Mankinen *et al.* (1985), the pre-gap direction is recorded by four flows (A46 to A43), and the post-gap direction by the flows A40 to A38, the latter having been briefly described above. In the present study, the thermal analysis of remanence was carried out in a similar fashion as for the first gap and the results are illustrated using the same modes of representation. As more material was available for the second gap than for the first one, we were able to carry out additional investigations aimed at identifying the remanence carriers of some critical flows. These investigations include microscopic observations of polished thin sections, electron microprobe analyses using a CAMEBAX probe, and thermal dependence of magnetic susceptibility measured using a Bartington bridge with a furnace allowing small rock fragments (approximately 2 g) to be heated under vacuum.

5.1 Pre-gap flows A43 and A42

5.1.1 Flow A43

Although the viscosity index v is extremely small (mostly between 1 and 2 per cent), and thus the Brunhes VRM

Downloaded from http://gji.oxfordjournals.org/ at ISTEEM /Institut des Sciences de la Terre de l'Eau et de l'Espace de Mont on February 19, 2013

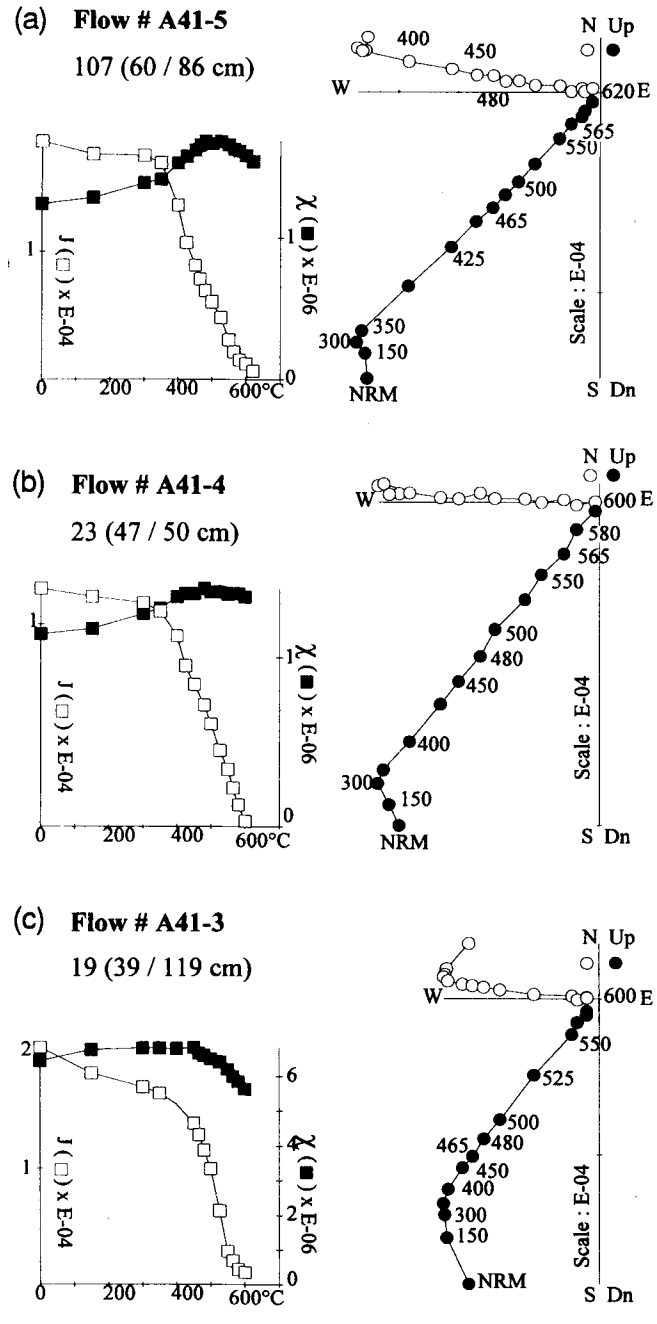

Figure 12. Thermal demagnetization of NRM for samples from flow A41-5 to A41-3. Same diagrams as in Fig. 2.

similarly negligible, almost all of the 21 cores from flow A43 carry a low-T low-coercivity remanence whose direction is sometimes very different from that found at high temperature (Figs 6 and 7). Almost all the specimens yield orthogonal demagnetization plots showing two distinct successive components defined by straight lines with an unusually sharp junction between them (Fig. 6c). We are dealing here with two components with the exceptional characteristic that both the unblocking temperature distributions and the unblocking field distributions of each magnetization component do not overlap. Because this anomalous behaviour could have provided us with some clues for some alternative, rock-magnetic interpretation of the palaeomagnetic observations relative to the overlying 'impulsive' flows A41-1 and A41-2 (see below), we decided to investigate the origin of the low-T low-coercivity component.

The high-temperature component, systematically defined from 400 °C to the Curie temperature, has the same direction throughout the flow thickness (Fig. 7). The average direction, which is not significantly different from that determined by AF demagnetization of the 1977 sampling of flow A43 (Table 1), corresponds to the pre-gap field direction, also recorded by three underlying flows (Mankinen *et al.* 1985). This component is evidently of primary origin.

The low-temperature component is characterized by an upper limit of the unblocking temperature interval equal to 400 °C, which is observed throughout the flow thickness. Similarly, the unblocking AF field range does not exceed 4 mT. Thus, this magnetization might be an IRM. This was verified by subjecting three specimens previously AF demagnetized to increasing dc fields. We found that a laboratory IRM having the same magnitude as that of the low-T low-coercivity component could be imparted to our specimens using dc fields between 2 and 4 mT. The destructive AF of these laboratory IRMs was found to vary between 2 and 5 mT, which agrees quite well with the coercivity of the low-T component.

Thermal variation of susceptibility under vacuum (χ–T curves) shows that, in agreement with the characteristics of the thermal demagnetization curves of NRM, a magnetic phase with an average Curie point close to 375 °C (determined by the method of Prévot *et al.* 1983) is present (Fig. 8). The decrease in susceptibility is rather abrupt, which indicates a magnetic carrier with a well-defined chemical composition. The sharpness of the angular changes on orthogonal diagrams (Fig. 6) is another expression of this chemical homogeneity. Such a Curie point could correspond to either some spinel or rhombohedral phase. Microscopic observations of polished thin sections from the central part of the flow and electron microprobe analyses of oxides showed that the magnetic minerals have two distinct origins. The first assemblage results from high-temperature oxidation of the originally high-titanium titanomagnetite phase which crystallized as rather large (up to 150 μm) euhedral grains. The less-oxidized crystals consist of ilmenite–titanomagnetite intergrowths of the trellis type (Haggerty 1976), and sometimes of the sandwich type too (Fig. 9a). In more-oxidized crystals, pseudobrookite (Pb_{ss}) and ilmenohaematite (Hem_{ss}) solid solutions develop at the expense of ilmenite and titanomagnetite (Fig. 9b) and ultimately constitute Pb_{ss}–Hem_{ss} intergrowths (Fig. 9c). Electron microprobe analyses show that the Hem_{ss} phases vary from almost pure haematite to titanohaematite with up to 20 per cent $FeTiO_3$ and that the Pb_{ss} phases correspond to fairly equal proportions of Fe_2TiO_5 and $FeTi_2O_5$. The latter phases have been reported to crystallize above 600 °C (Lindsley 1965).

The second assemblage derives from high-temperature oxidation of olivine (Haggerty & Baker 1967), and crystallized at the margins of this silicate (Fig. 9d) or in its proximity (Fig. 9e). According to electron microprobe analyses, the oxides formed are titanohaematite and spinel varying in composition from magnesian magnetite to magnesioferrite. The core of the olivine is dark with the exception of fine sympletic crystals which might be magnetite (Haggerty 1976). This kind of oxidation of olivine, accompanied by the transformation of titanomagnetite into an Hem_{ss}–Pb_{ss}

Downloaded from http://gji.oxfordjournals.org/ at ISTEEM /Institut des Sciences de la Terre de l'Eau et de l'Espace de Mont on February 19, 2013

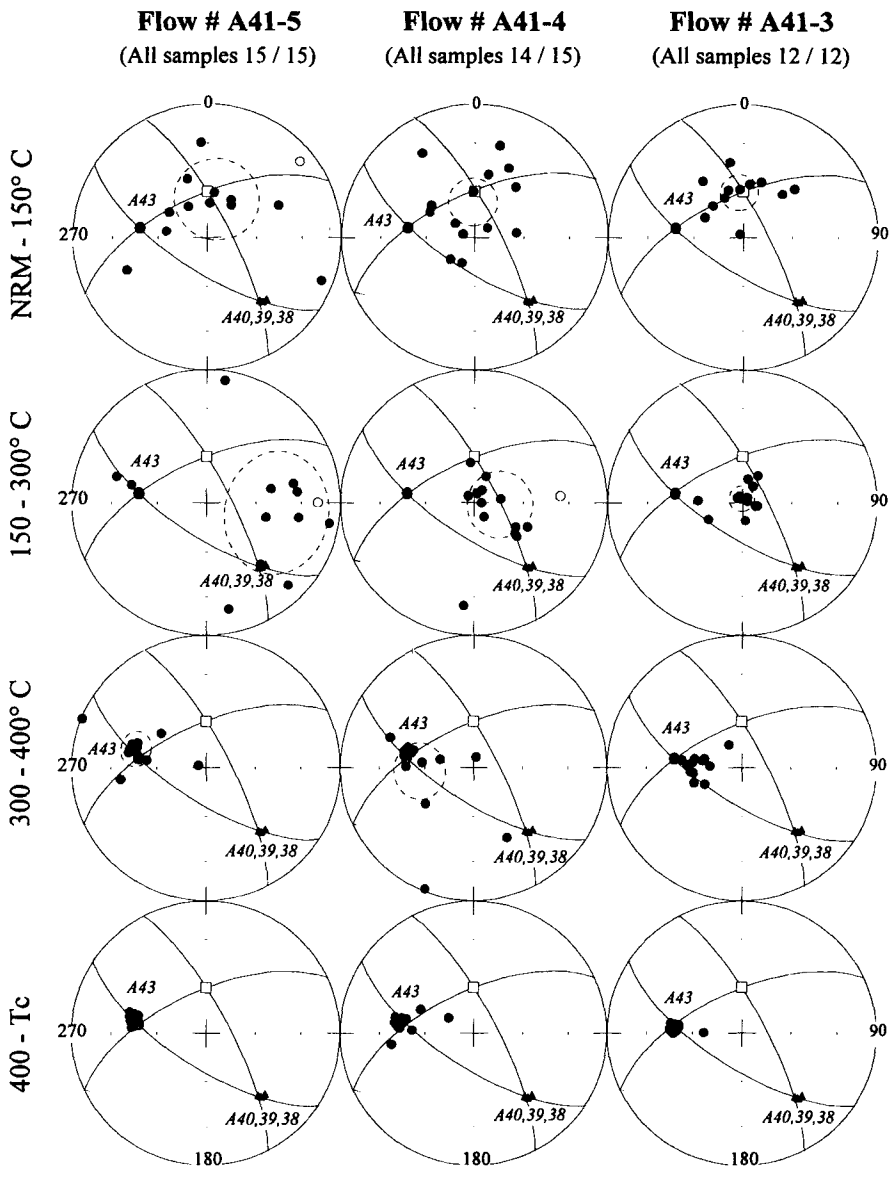

Figure 13. Equal-area projection of directions of vector differences calculated for different temperature intervals for all samples from flows A41-5, A41-4 and A41-3. Same diagrams as in Fig. 4. Dashed line represents the 95 per cent confidence cone about the average direction. Note that the evolution of the magnetization direction observed in these three flows requires at least three components (see text).

intergrowth, occurs above 600 °C according to both petrologic considerations (Haggerty 1976) and experimental data (Hoye & O'Reilly 1973).

Combining all these data, we conclude that three main magnetic phases are present in flow A43. Microchemical analyses indicate the presence of magnesioferrite, whose Curie temperature is close to 370 °C (Hoye & O'Reilly 1973). The χ–T curves show that this phase is more important in the central part of the flow where the low-coercivity IRM is particularly large (Fig. 8). Undoubtedly, magnesioferrite carries this IRM with unblocking temperatures lower than 400 °C. The thermal demagnetization curves of NRM (Fig. 8) suggest that the primary thermoremanent magnetization is carried by pure magnetite, probably mainly derived from olivine oxidation. As shown by Fig. 8, titanohaematite is a negligible magnetic carrier in terms of remanence, even though it is not so in terms of susceptibility: the phase with a Curie temperature close to 630 °C, which is particularly noticeable for specimens 85P071 and 85P080, can be attributed to a titanohaematite $y\mathrm{FeTiO_3}$, $(1\text{-}y)\mathrm{Fe_2O_3}$. According to Nagata & Akimoto (1956), this Curie temperature corresponds to $y=0.05$, which is compatible with the range of y values obtained from microchemical analyses.

5.1.2 *Flow A42*

This flow exhibits an ideally simple palaeomagnetic behaviour over its entire thickness. Orthogonal plots of thermal demagnetization are perfectly linear (Fig. 10a). There is no secondary component, thus no VRM. The directions of remanence do not show any trend with the vertical position of the core. They are well clustered (Fig. 10b) and provide an average in agreement with the previous determination for this flow (Table 1) and the four underlying ones (Mankinen *et al.* 1985).

Downloaded from http://gji.oxfordjournals.org/ at ISTEEM /Institut des Sciences de la Terre de l'Eau et de l'Espace de Mont on February 19, 2013

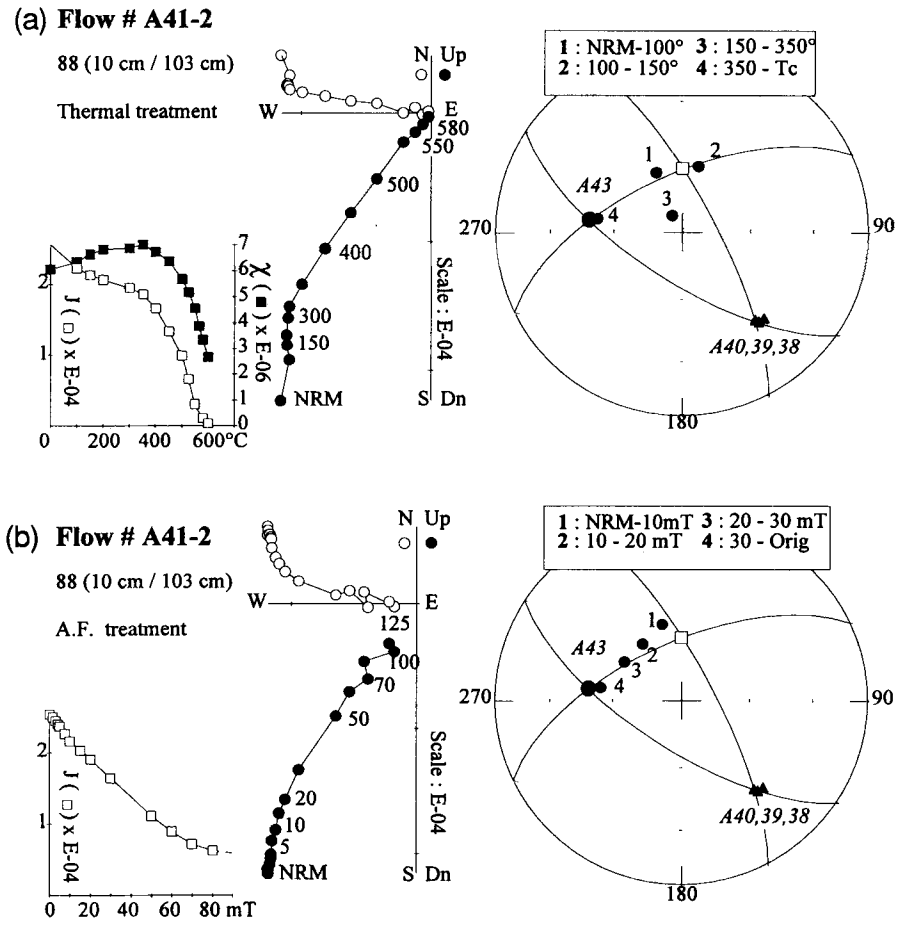

Figure 14. (a) Thermal and (b) AF demagnetization of NRM (left, □), room temperature susceptibility versus heating temperature (left, ■), orthogonal diagrams of progressive demagnetization of NRM (middle) and vector differences shown on an equal-area projection (right) for one sample from the bottom of flow A41-2. Same diagrams as in Fig. 2. A single magnetization throughout the thermal treatment beyond 300 °C and the AF treatment beyond 30 mT corresponding to the pre-jump direction is observed.

5.2 Flow units A41-5 to A41-1

The χ–T curves (Fig. 11) indicate that the magnetic mineralogy of these flows is dominated by high Curie temperature phases. Highly oxidized olivine crystals are observed in thin sections (J. M. Dautria, private communication), which suggests that these near-magnetite phases have the same origin as described for flow A43. These phases could not be identified more precisely because they are too small to be subjected to micro-chemical analyses. In contrast to flow A43, magnesioferrite, if present, does not represent a significant proportion of the magnetic minerals, since it does not show up on the χ–T curves (Fig. 11). Most of the titanomagnetite crystals show a feathery dentritic habit, even in the very central part of flow (Fig. 9f), which is characteristic of rapidly cooled magmas (Peck, Wright & Moore 1966; Kirkpatrick 1975). A similar magnetic mineralogy was observed in the stratigraphically equivalent thin flows D41 from site D, where rock-magnetic data suggest that magnetic carriers have a near single-domain size (Coe & Prévot, in preparation).

5.2.1 *Flows A41-5 to A41-3*

In all these three units, the main component of magnetization, which represents at least 80 per cent of the NRM and is observed from at least 400 °C to the Curie point (Fig. 11), has the same direction (Fig. 12), corresponding again to the pre-gap field (Table 1). The relative magnitude of the low-temperature component tends to increase from A41-5 to A41-3, although it remains small. As a result, the direction of these components is difficult to determine precisely. However, a significant trend is observed for each flow. The lowest temperature component (20–150 °C) is the same for all three flows. The direction cluster being relatively close to the direction of the axial dipole field (Fig. 13), this component has all the characteristics of a recent VRM. One would expect therefore that the difference vectors corresponding to the intermediate-temperature ranges 150–300 °C and 300–400 °C lie on the great circle between the pre-gap and the dipole directions, which is not the case (Fig. 13). Thus a third component is present in many of the specimens (see Hoffman & Day 1978), with some exceptions such as the two cores from the bottom of flow A41-5. There is little hope of determining the true direction of this third component, which is small and is moreover flanked by two other components whose unblocking temperature intervals may well partly overlap with that of the intervening component. However, the (scattered) directions for the 150–300 °C interval (Fig. 13) suggest for all three flows the existence of a component directed eastward to south-eastward of the pre-gap direction.

Downloaded from http://gji.oxfordjournals.org/ at ISTEEM /Institut des Sciences de la Terre de l'Eau et de l'Espace de Mont on February 19, 2013

© 1995 RAS, GJI 123, 484–506

Downloaded from http://gji.oxfordjournals.org/ at ISTEEM /Institut des Sciences de la Terre de l'Eau et de l'Espace de Mont on February 19, 2013

Table 2. Unusual magnetized flows.

Core Number	Distance (cm)	v %	Temperature Interval	δ	Inc	Dec	NRM Fraction
1st Gap : Flow # B51 (89 cm thick)							
85P224A	81	2.5	NRM-150	—	78.9	212.5	0.12
			150-300	—	55.5	314.0	0.12
			300-400	101.5	45.8	320.0	0.15
			400-500	100.0	47.3	320.0	0.24
			500-Tc	101.2	46.2	320.3	0.37
85P225A	78	2.0	NRM-150	—	75.2	343.8	0.14
			150-300	—	47.7	330.6	0.17
			300-400	100.3	47.5	325.0	0.19
			400-500	100.5	47.1	322.0	0.27
			500-Tc	99.1	48.5	321.8	0.24
85P226A	74	2.6	NRM-150	—	63.6	343.7	0.14
			150-300	—	55.9	339.4	0.17
			300-400	99.5	48.4	326.8	0.15
			400-500	92.9	55.0	324.9	0.25
			500-Tc	97.2	50.3	321.4	0.29
85P227A	71	2.2	NRM-150	—	72.1	280.5	0.15
			150-300	—	67.4	344.7	0.17
			300-400	82.8	64.5	348.8	0.16
			400-500	82.1	66.0	333.1	0.31
			500-Tc	83.4	64.7	331.3	0.20
85P228A	70	2.2	NRM-150	—	78.4	21.7	0.18
			150-300	—	65.2	349.6	0.17
			300-400	73.5	73.8	351.2	0.18
			400-500	83.0	65.1	332.4	0.30
			500-Tc	80.4	67.6	328.1	0.17
85P229A	64	4.2	NRM-150	—	80.6	320.5	0.20
			150-300	—	63.4	353.1	0.19
			300-400	75.8	72.1	341.6	0.13
			400-500	75.8	72.1	324.6	0.26
			500-Tc	78.7	69.1	321.3	0.22
85P230A	54	6.5	NRM-150	—	68.5	308.0	0.24
			150-300	—	70.3	355.6	0.19
			300-400	68.9	77.0	6.6	0.13
			400-500	79.8	68.2	331.7	0.27
			500-Tc	59.8	87.4	23.1	0.17
85P231A	54	5.8	NRM-150	—	74.6	321.7	0.21
			150-300	—	65.1	12.1	0.18
			300-400	71.7	72.7	11.8	0.14
			400-500	77.8	70.1	342.7	0.32
			500-Tc	47.1	78.2	131.0	0.15
85P232A	47	7.9	NRM-150	—	70.3	305.2	0.21
			150-300	—	69.2	354.1	0.20
			300-400	69.7	76.6	2.4	0.14
			400-500	80.0	68.1	329.2	0.33
			500-Tc	55.8	87.7	160.9	0.12

Table 2. (*Continued.*)

Core Number	Distance (cm)	v %	Temperature Interval	δ	Inc	Dec	NRM Fraction
85P233A	39	7.4	NRM-150	—	62.8	68.3	0.37
			150-300	—	58.5	58.9	0.18
			300-400	60.8	69.5	55.2	0.14
			400-500	69.1	63.8	39.5	0.25
			500-Tc	64.7	80.9	16.1	0.07
85P234A	33	18.9	NRM-150		57.0	113.0	0.29
			150-300	—	63.7	83.3	0.24
			300-400	50.1	75.0	93.7	0.16
			400-500	61.6	72.4	51.4	0.23
			500-Tc	59.6	88.4	349.3	0.08
85P235A	25	10.9	NRM-150	—	76.0	162.7	0.41
			150-300	—	61.7	87.8	0.23
			300-400	43.3	64.4	95.6	0.16
			400-500	54.9	81.9	85.2	0.15
			500-Tc	42.6	67.3	200.5	0.06
85P236A	14	—	NRM-150	—	87.6	145.4	0.36
			150-300	—	68.1	96.0	0.19
			300-400	49.4	80.7	172.8	0.11
			400-500	32.5	53.3	201.7	0.24
			500-Tc	32.1	33.4	223.0	0.11
85P237A	6	7.8	NRM-150	—	75.7	341.8	0.25
			150-300	—	72.2	63.4	0.18
			300-400	36.3	63.8	116.1	0.13
			400-500	16.6	47.7	137.7	0.27
			500-Tc	10.3	41.9	143.3	0.17
85P238A	6	6.7	NRM-150	—	72.8	139.0	0.25
			150-300	—	57.2	122.2	0.17
			300-400	13.9	45.5	142.7	0.13
			400-500	-15.8	16.1	142.1	0.28
			500-Tc	-21.1	10.9	147.6	0.18
2nd Gap : Flow # A41-2 (103 cm thick)							
85P084A	90	4.4	NRM-150	—	59.9	22.1	0.25
			150-300	—	63.9	33.6	0.18
			300-400	47.7	78.3	53.3	0.12
			400-500	34.4	80.1	269.7	0.17
			500-Tc	21.5	64.8	271.9	0.28
85P085A	63	5.7	NRM-150	—	61.6	336.5	0.36
			150-300	—	65.6	42.6	0.18
			300-400	54.6	77.1	86.6	0.11
			400-500	43.6	83.3	208.0	0.17
			500-Tc	23.7	64.3	262.5	0.17
85P086A	43	7.8	NRM-150	—	66.3	21.6	0.22
			150-300	—	71.9	69.4	0.16
			300-400	58.8	75.1	112.2	0.13
			400-500	38.4	79.2	237.6	0.19
			500-Tc	14.5	53.7	266.5	0.30

Table 2. (*Continued.*)

Core Number	Distance (cm)	v %	Temperature Interval	δ	Inc	Dec	NRM Fraction
85P087A	23	4.3	NRM-150	—	57.0	312.6	0.16
			150-300	—	75.3	39.7	0.12
			300-400	33.7	81.2	318.1	0.13
			400-500	22.0	66.8	276.9	0.21
			500-Tc	11.8	55.6	279.1	0.38
85P088A	10	2.4	NRM-150	—	62.5	344.9	0.18
			150-300	—	84.7	330.5	0.08
			300-400	17.7	65.2	292.9	0.11
			400-500	11.6	55.6	279.8	0.25
			500-Tc	7.6	50.6	278.9	0.38
85P089A	5	2.6	NRM-150	—	70.5	1.4	0.17
			150-300	—	77.4	7.4	0.09
			300-400	20.7	67.3	286.5	0.11
			400-500	11.0	53.9	276.9	0.22
			500-Tc	8.1	50.4	277.1	0.41
85P090A	4	2.4	NRM-150	—	60.5	353.7	0.14
			150-300	—	81.7	317.1	0.08
			300-400	19.9	64.2	276.2	0.12
			400-500	7.6	50.3	278.2	0.23
			500-Tc	6.9	48.9	276.6	0.42
2nd Gap : Flow # A41-1 (155 cm thick)							
85P135A	153	6.7	NRM-150	—	68.7	1.9	0.29
			150-300	—	54.0	126.9	0.15
			300-400	85.3	44.4	120.6	0.12
			400-500	82.6	47.1	120.4	0.19
			500-Tc	77.8	52.6	107.7	0.24
85P001A	135	5.4	NRM-150	—	69.8	15.6	0.30
			150-300	—	62.7	102.3	0.15
			300-400	69.9	58.8	126.0	0.10
			400-500	74.1	55.3	121.5	0.17
			500-Tc	70.0	59.2	121.6	0.27
85P002A	117	5.4	NRM-150	—	74.8	18.6	0.27
			150-300	—	70.3	83.9	0.17
			300-400	73.0	56.6	118.6	0.11
			400-500	65.4	61.7	136.5	0.22
			500-Tc	61.2	62.6	152.2	0.23
85P003A	105	8.0	NRM-150	—	65.6	12.3	0.31
			150-300	—	71.5	92.2	0.19
			300-400	62.4	66.4	104.4	0.12
			400-500	64.5	62.2	138.7	0.15
			500-Tc	54.2	68.9	160.0	0.22
85P004A	85	7.8	NRM-150	—	70.8	337.9	0.34
			150-300	—	74.2	16.8	0.21
			300-400	50.9	75.6	89.2	0.13
			400-500	66.9	60.2	136.3	0.19
			500-Tc	55.2	67.1	161.3	0.13

Table 2. (*Continued.*)

Core Number	Distance (cm)	v %	Temperature Interval	δ	Inc	Dec	NRM Fraction
85P005A	57	13.2	NRM-150	—	69.3	351.0	0.42
			150-300	—	69.1	48.2	0.21
			300-400	57.7	71.0	120.4	0.13
			400-500	60.7	68.0	123.5	0.14
			500-Tc	49.3	67.3	180.6	0.10
85P006A	37	9.4	NRM-150	—	74.3	332.5	0.32
			150-300	—	68.3	42.1	0.20
			300-400	56.5	72.0	108.5	0.12
			400-500	46.1	72.6	182.5	0.23
			500-Tc	30.9	67.4	229.9	0.13
85P007A	33	5.5	NRM-150	—	60.9	8.6	0.27
			150-300	—	74.8	60.9	0.14
			300-400	37.6	84.8	210.1	0.11
			400-500	22.3	74.1	279.5	0.20
			500-Tc	4.5	52.6	276.0	0.29
85P008A	13	6.2	NRM-150	—	61.6	0.2	0.34
			150-300	—	71.4	54.0	0.16
			300-400	53.7	74.3	131.6	0.09
			400-500	53.7	63.6	173.8	0.17
			500-Tc	34.7	58.5	218.0	0.23

Distance is measured from the bottom of the flow; v, viscosity index in per cent; interval of temperature where the direction is measured; δ, angular deviation from the pre-jump direction towards the post-jump direction; Inc, inclination; Dec, Declination.

Downloaded from http://gji.oxfordjournals.org/ at ISTEEM /Institut des Sciences de la Terre de l'Eau et de l'Espace de Mont on February 19, 2013

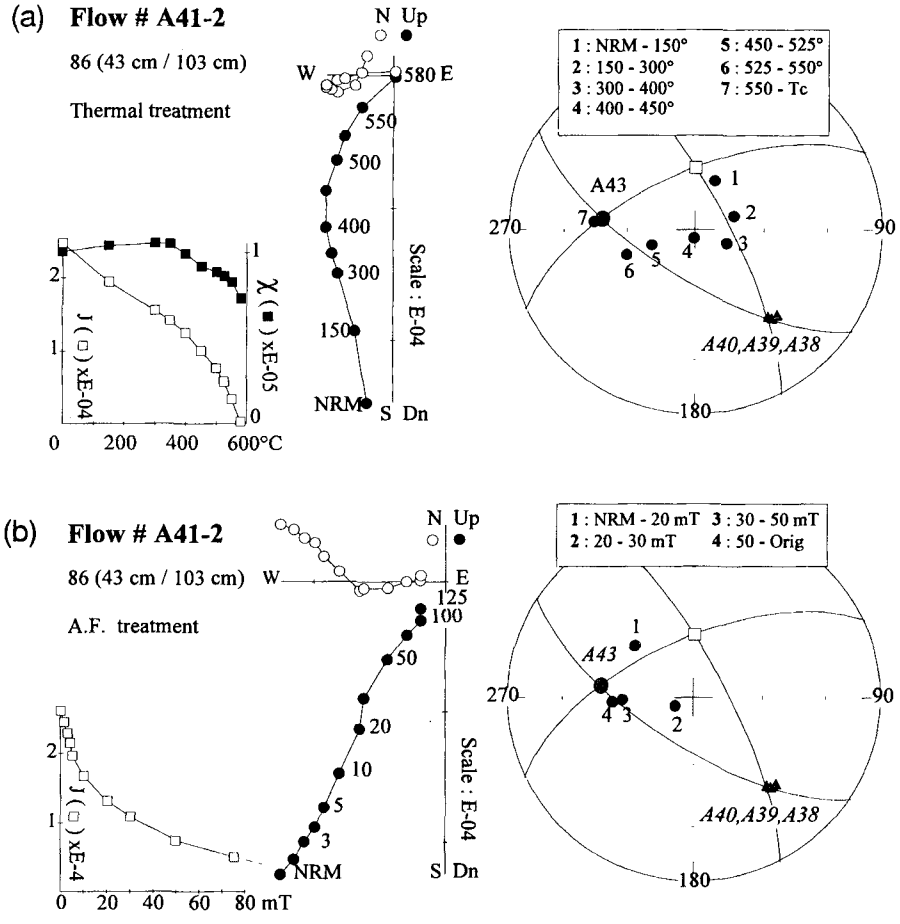

Figure 15. Sample from the middle of flow A41-2. Same diagrams as in Fig. 14. Note the continuous change in direction as the heating temperature or the AF is increased.

As we shall see below, such directions are also documented in the overlying flows.

5.2.2 *Flows A41-2 and A41-1*

Thermal and AF analyses of NRM revealed a more complex directional pattern, the directions being generally dependent on both the unblocking temperature (and field) and the vertical position of the core within the flow. Table 2 lists for each sample the direction for each temperature interval in which a significantly distinct remanence direction is observed.

For flow A41-2, the cores collected just above the bottom contact show a simple behaviour which can be explained by the presence of only two remanent components, easily distinguished by thermal treatment (Fig. 14a). The first component has unblocking temperatures ranging up to 350 °C and its direction is close to that of the dipole field. It is less selectively destroyed by AF (Fig. 14b). These characteristics suggest a Brunhes VRM. The second (and main) component shows the pre-gap direction and corresponds therefore to the primary TRM. For the specimens drilled higher in the flow (Figs 15 and 16), the direction of the difference vectors changes progressively with temperature from a low-T direction close to that of the present dipole field towards the pre-gap field direction at high-T. However, the intermediate-temperature directions do not lie on the great circle joining these two directions but instead approach the post-gap direction. AF demagnetization provides somewhat similar data, which indicates that the directional trend observed is real and is not an artefact due to magneto-mineralogical changes during heating. AF treatment is, however, much less efficient in unveiling distinct directions—an observation which favours a thermal origin of the magnetization components. As we will discuss below, the directions of these components are not only temperature-dependent for a given core, but also, for any given temperature interval, they depend on the vertical position of the core (Fig. 19).

In flow A41-1, two different kinds of behaviour are observed, depending on the vertical position of the core. The specimens collected within approximately 40 cm from the flow bottom (Figs 17b and c) behave qualitatively as observed for flow A41-2, although the direction of the intermediate difference vectors can sometimes come closer to the post-gap field direction (Table 2). For the cores higher in the flow, the change in direction with temperature is much simpler (Fig. 17a). After a VRM, well identified between room temperature and 150 °C (Fig. 18) over the entire flow thickness, is destroyed, the remanent direction remains approximately constant at higher temperature intervals. However, this direction is dependent on the vertical position of the core. The angular distance from

Downloaded from http://gji.oxfordjournals.org/ at ISTEEM /Institut des Sciences de la Terre de l'Eau et de l'Espace de Mont on February 19, 2013

the pre-gap direction increases as the top of the flow is approached (Fig. 19), the top two samples being magnetized approximately along the post-gap field direction (Fig. 18).

5.3 Summary of main observations

We can summarize as follows our main observations concerning the second directional gap as observed at site A.

(1) Flows A43 and A42 record only the pre-gap field direction.

(2) Flows A41-5 to A41-3 also record the pre-gap field direction; however, many samples carry in addition a weak remanence, unblocked at low temperatures (150–300 °C), which approaches the direction of some of the magnetization components found in the overlying flows.

(3) Flow A41-2 is characterized by a quite regular and unusual variation of partial remanent directions with temperature and vertical position of the rock sample within the flow. This unusual behaviour makes this flow an obvious candidate for having recorded a field change in direction during its cooling.

(4) The upper 1.0 m of flow A41-1 behaves as observed for the upper part of flow B51: the magnetization direction is basically constant with temperature but varies regularly with the distance from the top contact. The top exhibits a post-gap direction, then the direction turns progressively up to 30° towards the pre-gap direction when moving downwards. In contrast, the cores drilled closer to the base behave qualitatively as those from flow A41-2.

6 DISCUSSION

The previously reported detailed studies of the first and second directional gaps, respectively at sites B′ (Coe & Prévot 1989) and D (Camps *et al.* 1995; Coe *et al.* 1995), assume the occurrence of two processes:

(1) a thermochemical remagnetization of the upper part of the flow directly underlying the (first) post-gap flow(s); the remagnetized layer would have been some 80 cm thick in flow B51 at site B′ (Coe & Prévot 1989) and between 1.5 and 2 m at site D (Coe & Prévot, in preparation);

(2) a fast field change mainly recorded either in the same flow (B51 for the first jump at site B′) or in the underlying one (D41 for the second jump at site D).

A third process, a purely thermal or thermoviscous overprinting, was discarded as highly improbable (Coe *et al.* 1995; Coe & Prévot, in preparation). We will examine below the extent to which each of these mechanisms can account for the observations reported here.

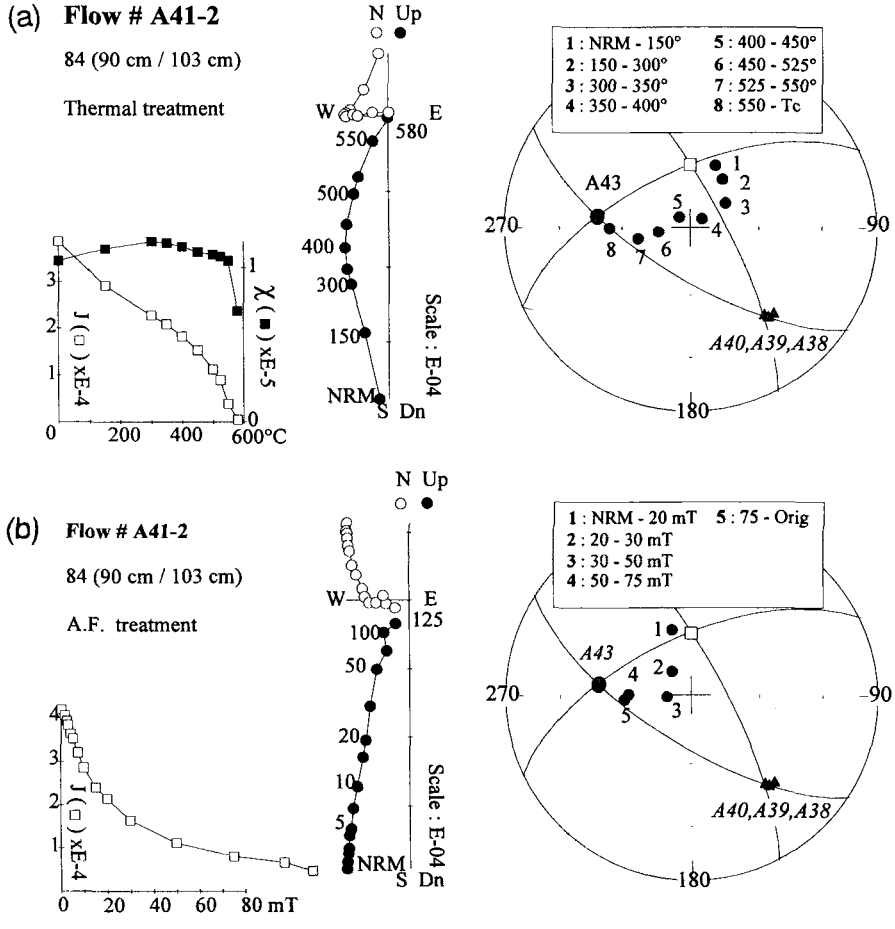

Figure 16. Sample from the top of flow A41-2. Same diagrams as in Fig. 14. Same observation as in Fig. 15. The magnetization direction is temperature-/AF-dependent.

Downloaded from http://gji.oxfordjournals.org/ at ISTEEM /Institut des Sciences de la Terre de l'Eau et de l'Espace de Mont on February 19, 2013

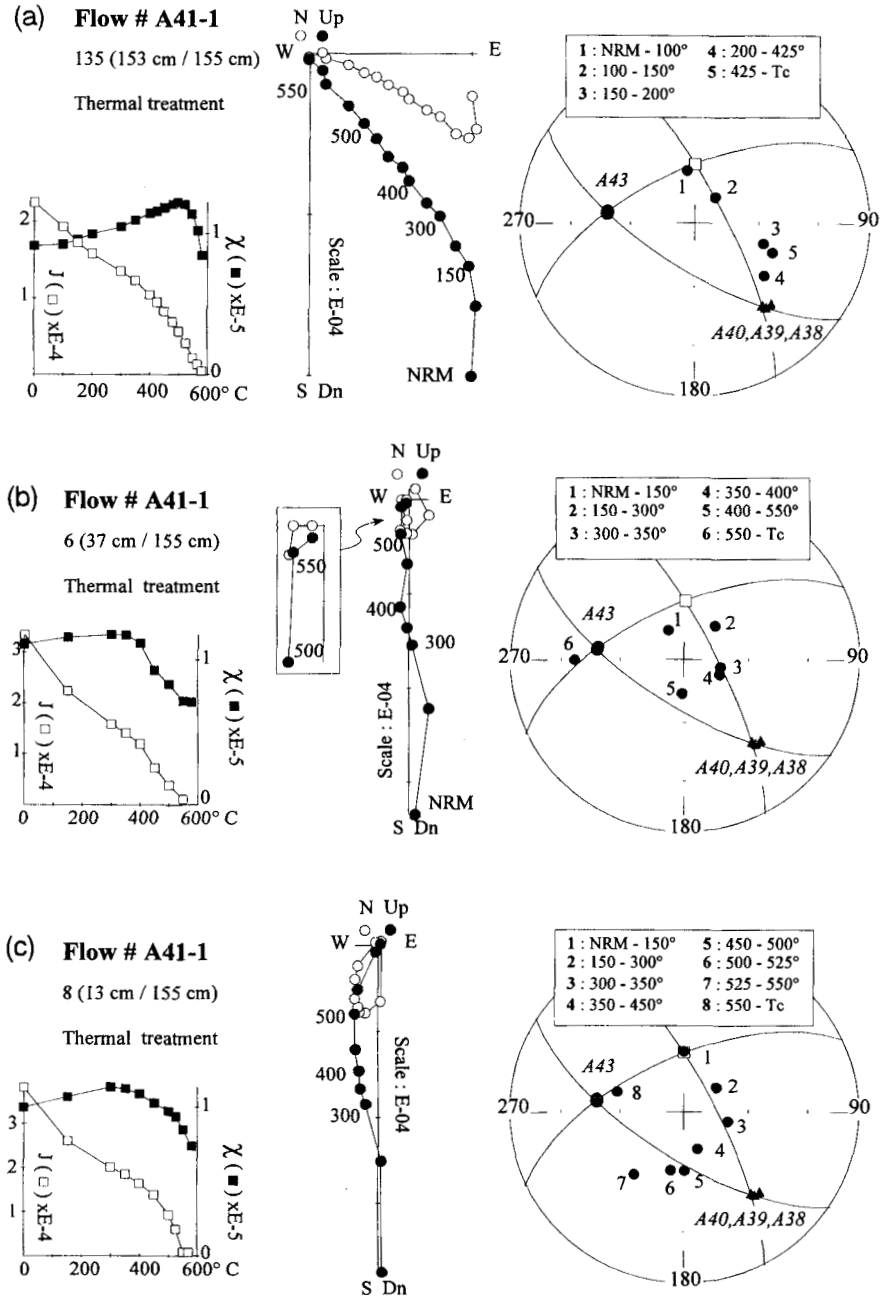

Figure 17. Sample from (a) the top, (b) the middle and (c) the bottom of flow A41-1. Same diagrams as in Fig. 14. A continuous change in magnetization direction as observed in the flow A41-2 is found in the lower part of this flow (b,c). On the other hand, the sample from the top (a) shows an approximately constant remanent direction throughout the thermal treatment beyond 200 °C.

6.1 Thermal or thermoviscous overprinting

By hypothesis, we deal here with a physical process immune from chemical effects. The physics of this kind of overprinting is well known, especially for single-domain or near single-domain grains such as the ones present in thin flows in which the initially fine titanomagnetite crystals have been further subdivided by exsolution lamellae (see above and Coe & Prévot, in preparation, for detailed rock-magnetic investigations). For a similar time of exposure to a given temperature, blocking and unblocking temperatures are the same (Néel 1955; Bol'shakov & Shcherbakova 1979; Dunlop & Ozdemir 1993) and the influence of time can be calculated from Néel's theory.

The value of baking temperature induced by a specific lava flow in nature is somewhat uncertain. The reference thermal model of Jaeger (1967) provides temperature estimates in the substratum which have been found to be much too high compared to the baking temperatures deduced from palaeomagnetic data (Audunsson & Levi 1988). An absence of any significant baking zone has even been reported for flows as thick as 100 m (Nyblade *et al.* 1987). Such palaeomagnetic observations seem to require a mode of volcanic emplacement with basal breccias representing the broken crust which has

Downloaded from http://gji.oxfordjournals.org/ at ISTEEM /Institut des Sciences de la Terre de l'Eau et de l'Espace de Mont on February 19, 2013

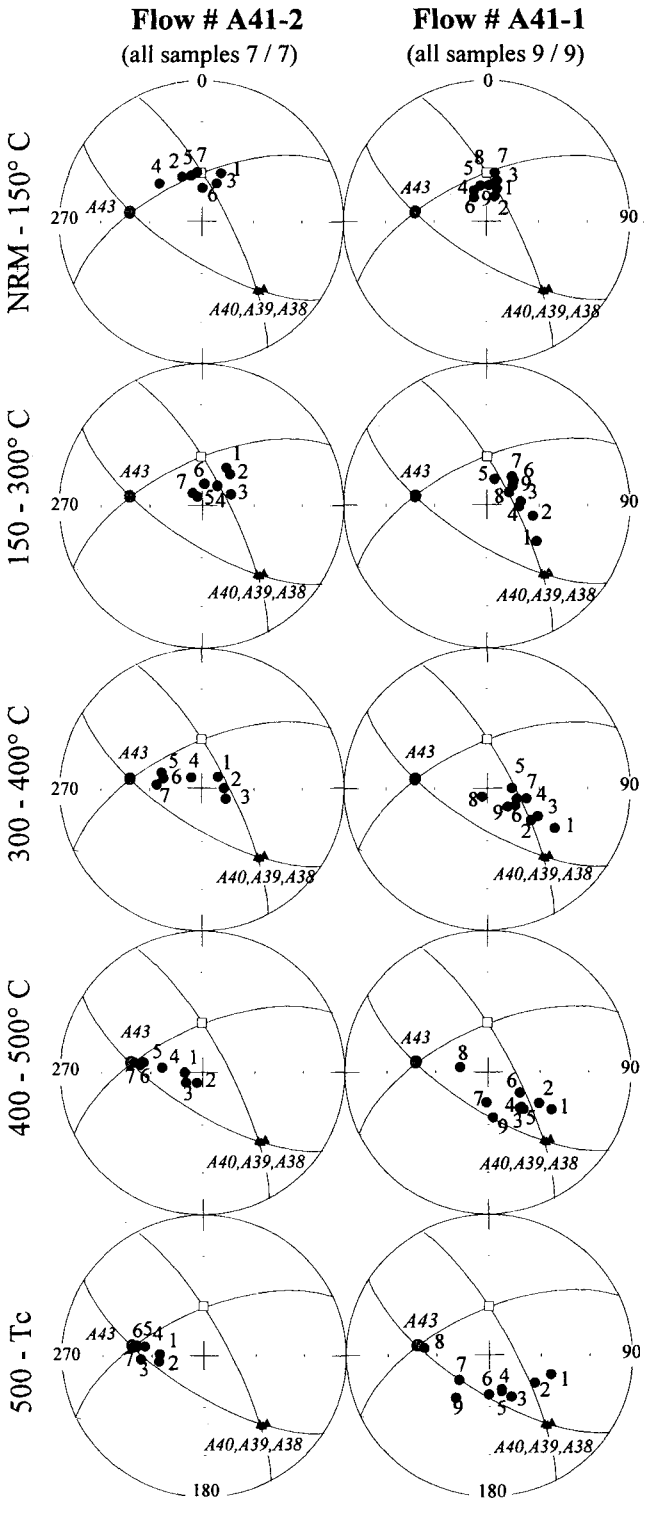

Figure 18. Equal-area projection of directions of vector differences calculated for different temperature intervals for all samples from flows A41-2 (left) and A41-1 (right). Same diagrams as in Fig. 4. For each flow, the numbering of the core starts at 1 and increases upward.

been overturned onto the flow base in tractor-tread fashion, and that have subsequently been reheated by the flowing magma and then welded (Stasiuk, Jaupart & Sparks 1993).

In order to examine more rigorously this possible thermoviscous overprint, we calculated the theoretical temperature profiles (Fig. 20) induced in the A41 units by the three overlying post-gap lava flows, assuming, for the reasons given above (Section 2), that they cooled successively. The model used, described in Camps *et al.* (1995), is a conductive model assuming an isothermal emplacement. This model probably provides a maximum temperature, particularly since the baked flows here are supposed to be entirely massive, without any vesicular zones. The interesting result is that the maximum reheating palaeotemperature in flow A41-1 has probably been imposed by flow A40, while it has been imposed by flow A38 in the underlying units. Also, the calculated reheating temperature in flows A41-3 to A41-5 is of the order of 300 °C, a temperature that would have been maintained for a few months. Taking into account the viscous effect as calculated by Dunlop & Ozdemir (1993), the unblocking temperature of this thermoviscous magnetization would have been close to 350 °C for flows A41-2 and A41-3 and hardly less for A41-4 and A41-5. Thus, the baking due to flow A38 can account for the component with eastward or south-eastward declination detected in flows A41-2 to A41-5 in the 150–300 °C temperature interval. Note that a slight contamination of the 300–400 °C vector difference by this post-gap remagnetization is clearly documented in flow A41-3 (Fig. 13). A similar contamination has to be suspected for flow A41-2 which is at the same level (Fig. 1). This implies that the angular displacement of magnetization direction towards the post-gap direction which is described in Fig. 19 is somewhat enhanced, in this temperature range, probably by some 10 °.

In contrast, a thermoviscous process cannot explain the progressive change of remanence direction with height which is observed in the upper part of B51 and A41-1. Fig. 21 shows that a thermoviscous effect would have resulted ideally in the angular deviation varying in a step-like function versus vertical distance, the step corresponding to each temperature interval being progressively offset downward as the unblocking temperature decreases. Obviously, this is not supported by experimental data.

6.2 Chemical or thermochemical overprinting

In contrast to thermoviscous remanence, the characteristics of chemical remanence cannot be constrained theoretically because they will depend on the specific chemistry (and possibly even size) of the phase undergoing transformation and the physicochemical conditions prevailing during this process. Thus, the constraints for interpreting our palaeomagnetic data can only be empirical. While most laboratory studies of CRM (chemical remanent magnetization) or TCRM (thermochemical remanent magnetization) deal with synthetic minerals or submarine basalts, Walderhaug (1992) reported thermochemical experiments relative to subaerial basalts, including a lava flow whose magnetic carrier is near-magnetite, formed after oxidation–exsolution of the original Ti-rich titanomagnetite, as found in the A41 units. The magneto-chemical changes due to heating in air at 525 °C under an applied field perpendicular to the NRM left were shown to result in a TCRM whose direction, fairly constant at higher temperatures, is intermediate between that of the NRM and the applied field.

Our data suggest that some overprinting by the post-gap flow occurs in the upper part of flows B51 and A41-1, within

Downloaded from http://gji.oxfordjournals.org/ at ISTEEM /Institut des Sciences de la Terre de l'Eau et de l'Espace de Mont on February 19, 2013

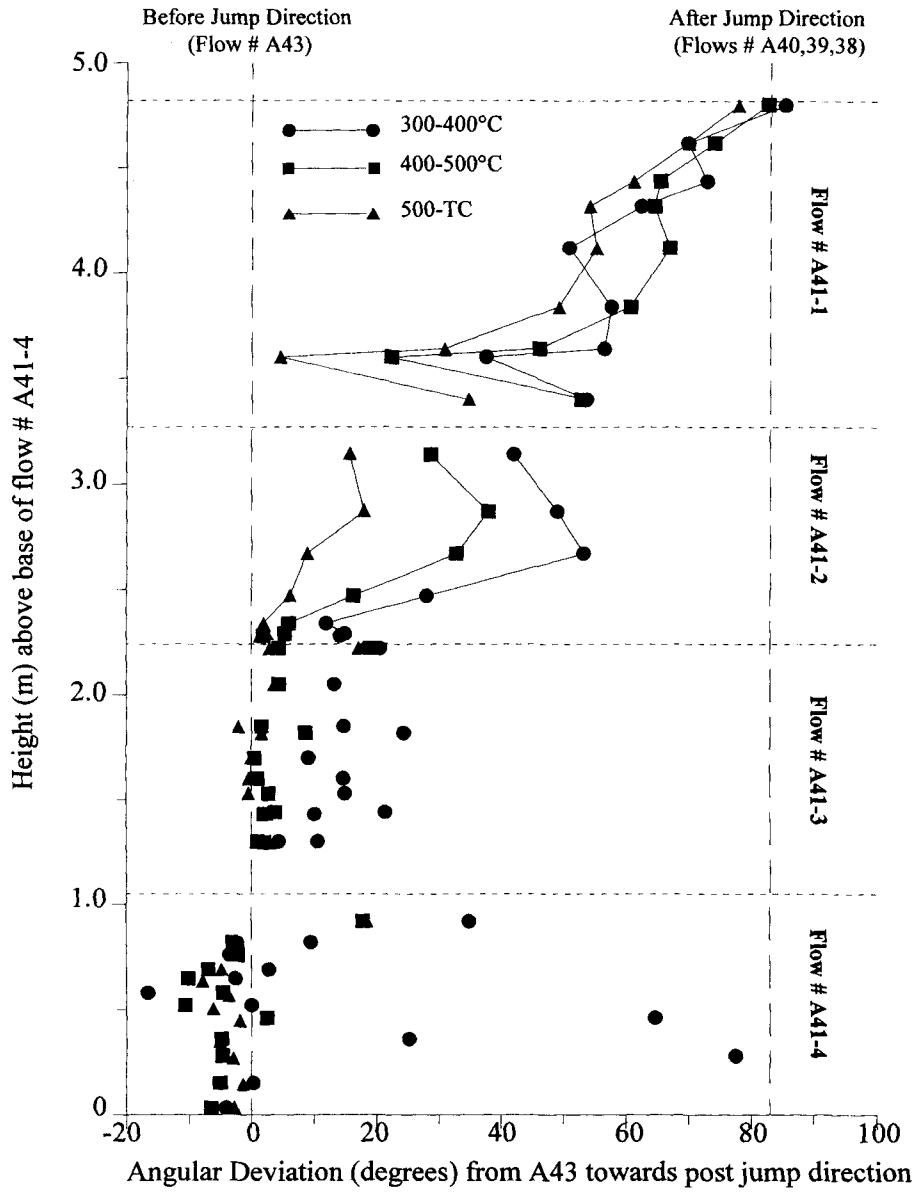

Figure 19. Angular deviation of remanence, calculated from the underlying (A43) towards the overlying flows A40–A38 direction, for different unblocking temperature intervals for samples from flows A41-4,3,2 and 1 as a function of their height above the base of flow A41-4. Same diagrams as in Fig. 5. Note the large swing in direction in flow A41-2 between the pre- and post-jump directions.

at least 70 cm and 1 m, respectively. Near the upper contact of these zones, the magnetization is entirely reset along the post-jump direction. Remagnetization effects decrease progressively downwards and become undetectable near the lower limit. Similarly, the results of the previous detailed study of flow B51 at site B′ (Coe & Prévot 1989) suggested a remagnetized layer of about 90 cm. A thermochemical remagnetization can be invoked for explaining the fact that the NRM directions in these zones are temperature-independent and intermediate between the pre- and post-gap directions. As the direction of magnetization in both flows is dependent on the distance from the upper contact (Figs 5 and 19), it would seem that the TCRM direction depends on the reheating temperature. We wish to point out that the actual reheating temperatures must have been lower (by at least 100–150 °C) than indicated by the thermal modelling (Fig. 20). This is attested to by the fact that low-temperature directions close to that of the post-gap flow direction are observed only within a few tens of centimetres from the upper contact, both in flows B51 and A41-1 (Figs 5 and 19).

Calling for a thermochemical overprinting in order to explain the palaeomagnetic observations for flow A41-2 is difficult. The NRM direction in this flow is strongly dependent on temperature, a behaviour that is not observed with laboratory TCRMs except for large overprinting fields (Walderhaug 1992). There is no petrological evidence for hydrothermalism in the interior of flow A41-2, as attested by the absence of any alteration of plagioclase and pyroxene crystals (J. M. Dautria, private communication). Thus, there does not seem to be any reason for this overprinting process to be maximum there, some 2 m below the stratigraphic contact with the post-gap flows.

Downloaded from http://gji.oxfordjournals.org/ at ISTEEM /Institut des Sciences de la Terre de l'Eau et de l'Espace de Mont on February 19, 2013

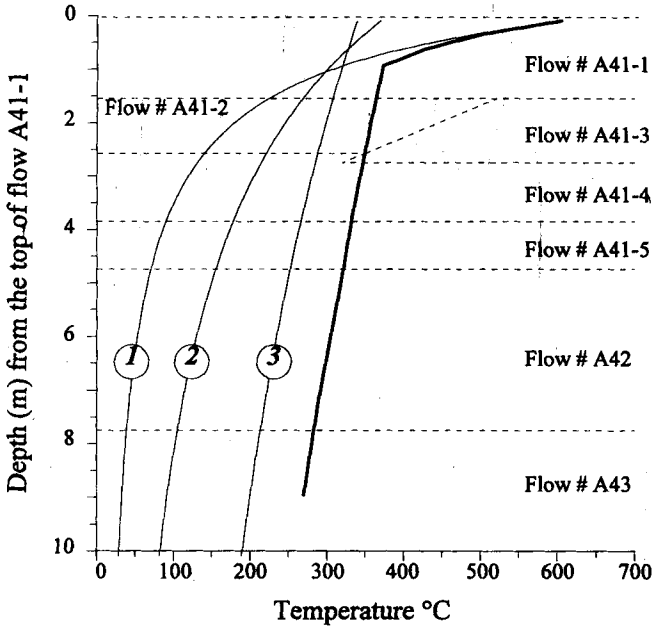

Figure 20. Maximum palaeotemperature profile induced in the A41, A42 and A43 units by the flow (1) A40, (2) A39 and (3) A38 assuming that they cooled successively. The heat transfer is computed numerically using the explicit cell balances method for a 1-D model (Shaw, Hamilton & Peck *et al.* 1977). The thick curve corresponds to the palaeotemperature profile corrected for the viscous effect according to Pullaiah *et al.* (1975).

6.3 Geomagnetic field changes during flow cooling

There is evidently no hope of recovering the original remanence of flow B51 which is remagnetized throughout most of its entire thickness (90 cm). Thus, it is not surprising not to be able to confirm the high-temperature trend in magnetization direction documented 25 m to the south at site B′ (Coe & Prévot 1989) where the thickness of this flow reaches almost 2 m. There, the diagnostic observations in favour of a field change during cooling found more than 1.2 m below the B51/B50 contact.

At site A, flow A41-2 is similarly remote from the critical contact with the overlying post-gap flows. This flow yields a vertical trend in angular deviation measured along the great circle from the pre-jump towards the post-jump direction (Fig. 19) which is qualitatively compatible with a progressive change in the field direction during the flow cooling. The directions obtained from the cores from the middle of the flow being closer to the post-gap direction, we obtain a 'belly'-shaped profile, as previously reported for the first impulse at site B′ (Coe & Prévot 1989) and for the second impulse at site D (Coe *et al.* 1995). Such a shape is qualitatively compatible with the isotherms that describe the evolving temperature distribution in a cooling lava flow. The similarity of the trends for the three temperature intervals considered and their progressive offset with respect to each other also are compatible with a shift in field direction during cooling of the flow. This compatibility has been verified. Using the same cooling model as for the equivalent flow D41 at site D (Camps *et al.* 1995), we calculated the blocking times (measured from the beginning of flow cooling) corresponding to the unblocking temperatures of the complete set of remanence directions obtained from all

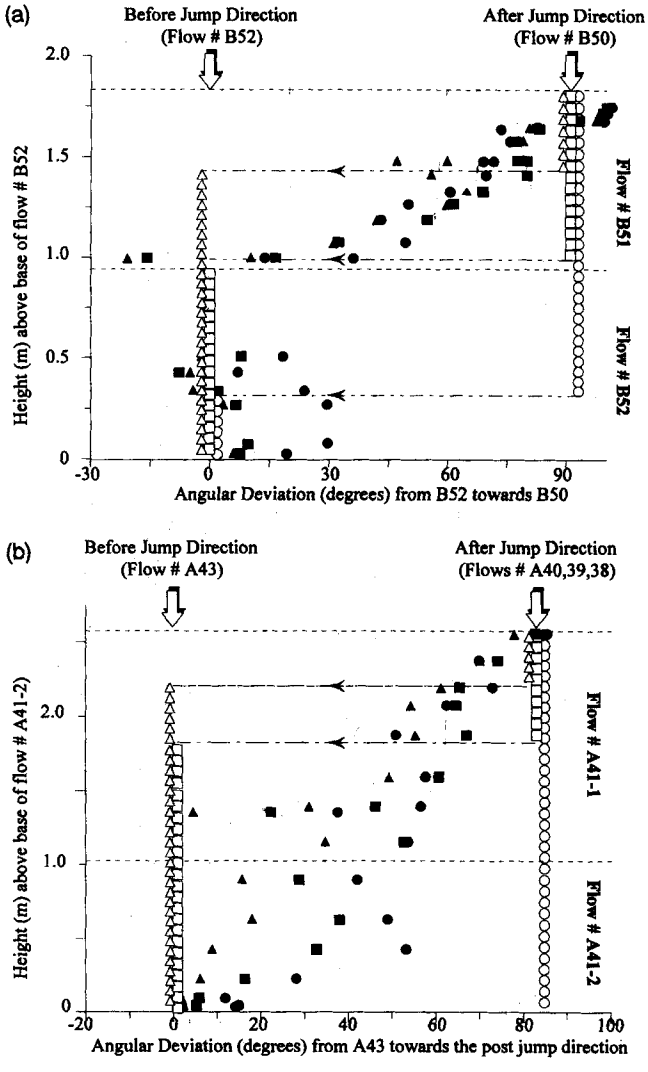

Figure 21. Angular deviation of remanence calculated for different unblocking temperature intervals for (a) the first and (b) the second jump. Circles, squares and triangles correspond to the direction calculated in the 300–400 °C, 400–500 °C and 500-T_c temperature intervals respectively. Open symbols correspond to the theoretical distribution of direction according the hypothesis of a thermal or thermoviscous overprint guided by the maximum temperature profile calculated as in Fig. 20.

cores. This calculation assumes that blocking and unblocking temperatures are the same. There is a clear correlation between angular deviation and time, especially if, as in Fig. 22, flow A41-1 is supposed to have been emplaced only a few hours after A41-2. This latter hypothesis is compatible with the volcanological observations reported above (Section 2), suggesting that flows A41 all belong to the same eruptive episode. It is also in agreement with the observations (Section 5.2) that the cores from the top of flow A41-2 and the bottom of flow A41-1 behave somewhat similarly, both sets showing a large and rather similar change of remanence direction versus temperature. According to the geomagnetic change hypothesis, this behaviour indicates a rather slow cooling on both sides of the contact between these flows. This hypothesis is also reasonable from a volcanologic standpoint, because distinct pahoehoe flow boundaries like those separating each of the

Downloaded from http://gji.oxfordjournals.org/ at ISTEEM /Institut des Sciences de la Terre de l'Eau et de l'Espace de Mont on February 19, 2013

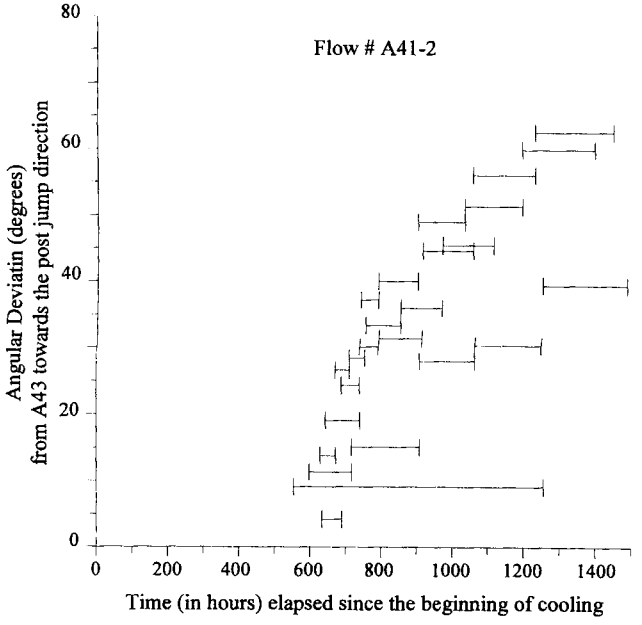

Figure 22. Angular deviation of the directions obtained from flow A41-2, calculated from the underlying (A43) towards the overlying flows (A40–A38) direction, and plotted against the time elapsed since the beginning of cooling. For each sample, several data are generally plotted, each of them corresponding to a temperature interval in which the direction of the vector difference remains constant (Camps *et al.* 1995). The bar indicates the cooling time interval during which each direction of magnetization was blocked. In this calculation, we assume that the flow A41-1 was emplaced just 10 hr after flow A41-2.

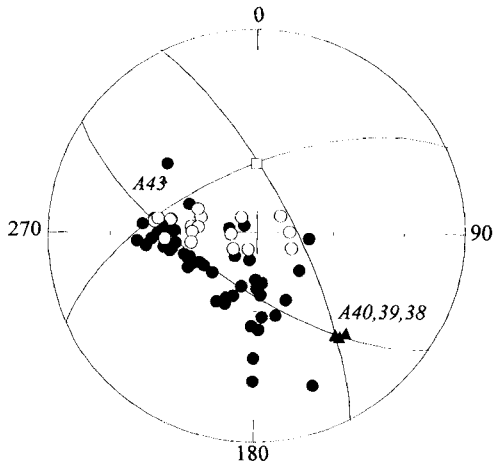

Figure 23. Comparison of the magnetization direction measured in flow A41-2 (○, this study) with the direction measured in flow D41 (●, section D, see Fig. 1 and Coe *et al.* 1995; Camps *et al.* 1995).

flows in the sequence A41 can be observed, even with a time interval between emplacement of individual units as short as one hour (G. P. Walker, private communication).

The correlation observed between angular deviation and time is an argument in favour of the geomagnetic change hypothesis. The rate of change of the field deduced from Fig. 22 is 2°–3° per day, which is in reasonable agreement with the figure obtained from flow D41 at site D (6°±2° per day; Camps *et al.* 1995). Taking into account the palaeointensity estimates from the adjacent flows (≈7 μT; see Table 1), the corresponding change of the field vector is found to be equal to 250–350 nT per day.

However, a rather puzzling disagreement exists between the data obtained for the second impulse at sites A and D. As shown in Fig. 23, the field directions move eastwards away from the pre-jump direction at site A while they move south-eastwards according to the data obtained from site D (Coe *et al.* 1995; Camps *et al.* 1995). Although flow A41-2 at site A and flow D41 at site D, 250 m north, are not necessarily the same (the outcrop is somewhat discontinuous between these two sites), they are at the very same stratigraphic level: they both correspond to the second aphyric flow below the bottom of the easily followed porphyritic flow sequence exhibiting post-jump directions. Therefore units A41-2 and D41, even if distinct from each other, cannot reasonably be supposed to have recorded two different impulses. There is, of course, no reason why the geomagnetic field direction during the impulse should follow the great circle between the pre- and post-directions. But the directional path, whatever it is, has to be the same at both sites. Considering the geometry of the three field directions which can interfere (Figs 13 and 18), a systematic difference in magnetic viscosity between these two sites seems *a priori* a possible explanation, the more so since the directions which are the farthest from the pre-jump field correspond in general to the lowest temperature intervals. However, viscosity index measurements were not found to be significantly larger for flow A41-2 than for flow D41 (Table 2). Thus, additional sampling and experiments seem necessary to explore the origin of this discrepancy.

7 CONCLUSIONS

This reinvestigation of the sites where the occurrence of geomagnetic field impulses was first suspected (Mankinen *et al.* 1985; Prévot *et al.* 1985a, b) led us to somewhat different conclusions for the first and the second impulses. At site B (first impulse), we find that the dependence of the remanence direction on the sample vertical position in flow B51 does not imply a directional field change during flow cooling, but is better explained by a thermochemical overprinting due to the overlying B50 flow. However, this conclusion does not challenge the existence of the first impulse because this field change seems to have been recorded some 25 m away in flow B51 (Coe & Prévot 1989), at a place where this flow is thick enough for the record of the impulse not to have been erased by the baking due to B50.

Regarding the second impulse, restudied at site A, our new findings are more comprehensively explained by a change in the field direction during cooling of flow A41-2 than by some overprinting. Using a simple model of flow cooling, the angular rate of change of the field is estimated to have been of the order of 2°–3° or 250–350 nT per day during the impulse. This figure is similar to that obtained from site D, some 250 m away. However, the directional paths describing the field change are somewhat different at both sites. Several new sites, up to 2 km apart from each other, were intensively sampled last summer in order to investigate the significance of this discrepancy.

ACKNOWLEDGMENTS

We thank Greg Baker for his help for the 1985 sampling, and J. M. Dautria (University of Montpellier) and M. Leblanc

Downloaded from http://gji.oxfordjournals.org/ at ISTEEM /Institut des Sciences de la Terre de l'Eau et de l'Espace de Mont on February 19, 2013

(Centre National de la Recherche scientifique) for their help with microscopic observations. We particularly wish to acknowledge George P. L. Walker, from the University of Hawaii, for visiting the sites of the second impulse last summer, and allowing us to benefit from his great experience in volcanology. We also greatly appreciate the help given by E. Herrero-Bervera, E. Cañón-Tapia and J. Glen during our last field trip. The comments of P. Roperch and an anonymous reviewer are appreciated. This work was partially funded by CNRS-INSU, Programme 'Dynamique et Bilan de la Terre No. 2, Terre Profonde', contribution No. 15 and by NATO (grant CRG 940215).

REFERENCES

Audunsson, H. & Levi, S., 1988. Basement heating by a cooling lava: paleomagnetic constraints, *J. geophys. Res.*, **93**, 3480–3496.

Bol'shakov, A.S. & Shcherbakova, V.V., 1979. Thermomagnetic criterion for determining the domain structure of ferrimagnetics, *Izv. Akad. Nauk SSSR*, **15**, 111–117.

Camps, P., Prévot, M. & Coe, R.S., 1995. The hypothesis of transitional geomagnetic impulses: Combining paleomagnetic data with a cooling model of lava flows, *C. R. Acad. Sci. Paris*, t.320, Série IIa, 801–807.

Coe, R.S. & Prévot, M., 1989. Evidence suggesting extremely rapid field variation during a geomagnetic reversal. *Earth planet. Sci. Lett.*, **92**, 292–298.

Coe, R.S., Prévot, M. & Camps, P., 1995. New evidence concerning impulsive field change during a geomagnetic reversal, *Nature*, **374**, 687–692.

Dunlop, D.J. & Ozdemir, O., 1993. Thermal demagnetization of VRM and pTRM of single domain magnetite: no evidence for anomalously high unblocking temperatures, *Geophys. Res. Lett.*, **20**, 1939–1942.

Fuller, M., 1989. Fast changes in geomagnetism, *Nature*, **339**, 582–583.

Gubbins, D. & Roberts, P.H., 1987. Magnetohydrodynamics of the Earth's core, in *Geomagnetism*, pp. 51–61, ed. Jacobs, J.A., Academic Press, London.

Haggerty, S.E., 1976. Oxidation of opaque mineral oxides in basalts, in *Oxide Minerals*, pp. Hg1–Hg277, ed. Rumble, D., Blacksburg.

Haggerty, S.E. & Baker, I., 1967. The alteration of olivine in basaltic and associated lavas. Part 1: High temperature alteration, *Contrib. Mineral. Petrol.*, **16**, 233.

Hoffman, K.A. & Day, R., 1978. Separation of multi-component NRM: a general method, *Earth planet. Sci. Lett.*, **40**, 433–438.

Hoye, G.S. & O'Reilly, W., 1973. Low temperature oxidation of ferromagnesian olivines. A gravimetric and magnetic study, *Geophys. J.R. astr. Soc.*, **33**, 81–92.

Jaeger, J.C., 1967. Cooling and solidification of igneous rocks, in *Basalts (2)*, pp. 503–536, eds Hess, H.H. & Poldervaant, A., Interscience, New York, NY.

Kirkpatrick, R.J., 1975. Crystal growth from the melt: a review, *Am. Mineral.*, **60**, 798–814.

Langel, R.A. & Estes, R.H., 1985. The near-earth magnetic field at 1980 determined from Magsat data, *J. geophys. Res.*, **90**, 2495–2509.

Lévêque, F., 1992. Confrontation des données biochronologiques et magnétostratigraphiques dans les gisements continentaux du paléogène européen. Etalonnage temporel de l'échelle biochronologique mammalienne, *Diplome de doctorat*, Univ. Montpellier II, France.

Lindsley, D.H., 1965. Lower thermal stability of $FeTi_2O_5$-$Fe_2Ti_0$5 (pseudobrookite) solid solution series (abstr), *Progr. Ann. Meet. Geol. Soc. Am.*, **96**.

Mankinen, E.A., Prévot, M., Grommé, C.S. & Coe, R.S., 1985. The Steens Mountain (Oregon) geomagnetic polarity transition. 1. Directional history, duration of episodes, and rock magnetism, *J. geophys. Res.*, **90**, 10 393–10 416.

Nagata, T. & Akimoto, S., 1956. Magnetic properties of ferromagnetic ilmenites, *Geofis. Pura Appl.*, **34**, 36–50.

Néel, L., 1955. Some theoretical aspects of rock magnetism, *Adv. Phys.*, **4**, 191–241.

Nyblade, A.P., Shive, P.N. & Furlong, K.P., 1987. Rapid secular variation recorded in thick Eocene flows from the Absaroka Mountains of northwest Wyoming. *Earth planet. Sci. Lett.*, **81**, 419–424.

Peck, D.L., Wright, T.L. & Moore, J.G., 1966. Crystallization of tholeiitic basalt in Alae lava lake, Hawaii, *Bull. Volcanol.*, **29**, 629–656.

Prévot, M., 1975. Magnétisme et minéralogie magnétique de roches néogènes et quaternaires, contribution au paléomagnétisme et à la géologie du Velay, *Thèse d'état*, Pierre et Marie Curie, Paris, France.

Prévot, M., Mankinen, E.A., Grommé, C.S. & Lecaille, A., 1983. High paleointensities of the geomagnetic field from thermomagnetic studies on rift valley pillow basalts from the mid-Atlantic ridge. *J. geophys. Res.*, **88**, 2316–2326.

Prévot, M., Mankinen, E.A., Coe, R.S. & Grommé, C.S., 1985a. The Steens Mountain (Oregon) geomagnetic polarity transition. 2. Field intensity variations and discussion of reversal models, *J. geophys. Res.*, **90**, 10 417–10 448.

Prévot, M., Mankinen, E.A., Grommé, C.S. & Coe, R.S., 1985b. How the geomagnetic field vector reverses polarity, *Nature*, **316**, 230–234.

Pullaiah, G., Irving, E., Buchan, K.L. & Dunlop, D.J., 1975. Magnetization changes caused by burial and uplift, *Earth planet. Sci. Lett.*, **28**, 133–143.

Shaw, H.R., Hamilton, M.S. & Peck, D.L., 1977. Numerical analysis of lava lake cooling models: Part I, Description of the method, *Am. J. Sci.*, **277**, 384–414.

Stasiuk, M.V., Jaupart, C. & Sparks, R.S., 1993. Influence of cooling on lava-flow dynamics, *Geology*, **21**, 335–338.

Thellier, E. & Thellier, O., 1944. Recherches géomagnétiques sur les coulées volcaniques d'Auvergne, *Ann. Geophys.*, **1**, 37–52.

Walderhaug, H., 1992. Directional properties of alteration CRM in basic igneous rocks, *Geophys. J. Int.*, **111**, 335–347.

Walker, G.P.L., 1970. Compound and simple lava flows and flood basalts, *Bull. Volcanol.*, **35**, 579–590.

Downloaded from http://gji.oxfordjournals.org/ at ISTEEM /Institut des Sciences de la Terre de l'Eau et de l'Espace de Mont on February 19, 2013